Available online at www.sciencedirect.com
SCIENCE DIRECT
Precambrian Research 147 (2006) 366–386
Precambrian Research
www.elsevier.com/locate/precamres

Birth of a volcanic passive margin in Cambrian time: Rift paleogeography of the Ossa-Morena Zone, SW Spain

Maider Etxebarria [a,*], Françoise Chalot-Prat [b], Arturo Apraiz [a], Luis Eguíluz [a]

[a] *Dpto. de Geodinámica, Fac. de Ciencias y Tecnología, EHU/UPV, Apdo 644, 48080 Bilbao, Spain*
[b] *CRPG-CNRS/Nancy University, BP 20, 15 rue Notre Dame des Pauvres, 54501 Vandoeuvre, France*

Received 20 December 2004; received in revised form 22 September 2005; accepted 6 January 2006

Abstract

Mapping at 1:10000 scale of both north (N) and south (S) flanks of the Variscan Monesterio antiform in the Ossa-Morena Zone (southern Spain), in association with detailed petrographic and major element analyses of magmatic rocks has revealed the building of a passive, but volcanically active, oceanic margin in Cambrian time. This margin was located in northern Gondwana and represents the beginning of an extensional tectonic regime that concluded with the opening of the Rheic Ocean. At time of eruption (Middle Cambrian), the N flank was located on the northern coastline of a marine basin in the process of passive rifting. The vents, mainly located in its western part, were subaerial continental and/or shallow marine. On the S flank, eruptions and deposits were shallow marine, occurring as lava flows and pillows interstratified within shallow marine sediments. On both flanks, intrusives were emplaced after the extrusives. Lateral thickness variations of the sedimentary deposits testify to the building, during four distinct periods, of a rifted passive margin with a shifting locus of volcanic activity over time. The composition of magmas was bimodal. The mafic magmas are silica-saturated, alkaline to sub-alkaline and somewhat Ti-rich, perhaps originating from partial melting of a subcontinental mantle that was less metasomatized with time. The youngest magmatism, with an affinity close to that of MORB, likely had an asthenospheric source. The alkaline felsic products are diverse and may have originated from a very heterogeneous continental crust. In each set, partial melting relationships prevail, suggesting that the melts rose along open fractures as soon as they formed. In the context of lithospheric thinning, it is possible that mantle and crustal melting was triggered by decoupling between rheologically different materials.

Keywords: Volcanism; Passive oceanic margin; Petrography; Geochemistry; Cambrian; Variscan cycle; Ossa-Morena Zone; SW Spain

1. Introduction

This study mainly concerns the eruptive dynamics and the composition of Middle Cambrian volcanics, and their relationships with the tectono-sedimentary setting prevailing before, during and after the eruptions. Intrusive rocks, emplaced during that period, are also examined. The geodynamic context of eruptions was post-collisional and predated the opening of the Rheic Ocean (Sánchez García et al., 2003 and references therein).

One aim was to better understand both the Cadomian (or Pan-African) post-collisional context and the earliest steps of the Variscan orogenic cycle in the western part of Europe (Ossa-Morena Zone, SW Spain). There is general agreement that the Ossa-Morena Zone, like other fragments of the Cadomian-Avalonian orogen (North Armorica and parts of the Bohemian Massif of Central Europe) were deposited in the northern Gondwana margin, adjacent to the West African craton (Friedl et al., 2000; Tichomirowa et al., 2001; Fernández-Suárez

* Corresponding author.
E-mail address: npbetakm@lg.ehu.es (M. Etxebarria).

0301-9268/$ – see front matter © 2006 Published by Elsevier B.V.
doi:10.1016/j.precamres.2006.01.022

et al., 2002). At the end of the Neoproterozoic subduction along the margin changed progressively into a transform regime, producing the tectonic amalgamation that generated the Armorica Terrane Assemblage (Murphy et al., 2000; Fernández-Suárez et al., 2000; Gutíerrez-Alonso et al., 2003). Overlapping this phase of transform regime the beginning of an extensional process took place, which finished with the opening of the Rheic Ocean between Avalonia and the Armorica Terrane Assemblage (Sánchez García et al., 2003; Murphy et al., 2004).

The study of such extrusive and intrusive magmatism, is interesting inasmuch as it provides a tracer not only of the rheological behavior of the continental lithosphere during the earliest, extensional stage of an orogenic cycle, but also of the composition of the mantle and continental crust susceptible to partial melting during this period.

The orogenic cycle begins either by a lasting crustal thinning, that leads to seafloor spreading, or by a transient crustal thinning immediately followed by doming of the thinned continental lithosphere due to isostatic compensation (Boillot and Coulomb, 1998). In both settings, magmas can be emplaced within or/and upon the continental crust.

Mafic volcanics vary in composition from continental tholeiitic flood basalts in the first type of context, to alkaline and even calc-alkaline basalts within the second type (Wilson, 1989; Foley, 1992; Chalot-Prat and Boullier, 1997; Pecerillo, 1999; Pecerillo and Panza, 1999; Chalot-Prat and Girbacea, 2000; Best and Christiansen, 2001; Winter, 2001; Mc Cann et al., 2003). This magmatism reflects partial melting of a subcontinental mantle, more or less metasomatized during previous subduction- and collision-related events (Chalot-Prat and Boullier, 1997; Pecerillo, 1999; Pecerillo and Panza, 1999). The continental tholeiitic affinity attests to a much less metasomatized mantle source composition close to that of the asthenosphere, the source of Mid-Oceanic Ridge Basalts (MORB). In addition, the presence of felsic volcanism, may signal partial melting of the overlying continental crust (Wilson, 1989; Chalot-Prat, 1995; Best and Christiansen, 2001).

In southern Spain, Cambrian volcanics and related sediments reflect the occurrence of bimodal alkaline magmatism in a subaerial to shallow marine continental rifting setting (Bard, 1969; Mata and Munhá, 1986, 1990; Liñán and Quesada, 1990; Sagredo and Peinado, 1992; Giese and Bühn, 1993; Sánchez-Carretero et al., 1999; Sánchez García et al., 2003).

Another aim of our work was to characterize the diversity in space and time of volcanic lithologies in order to identify the eruptive dynamics, the conditions of accumulation of volcanic products, the location of vents, and the composition of the different magmas and of their possible sources. A detailed mapping at 1:10000 scale was carried out on both flanks (Zafra-Nogales and Jerez de los Caballeros) of a Variscan antiform of the Ossa-Morena Zone (Fig. 1). A previously undocumented large variety of Cambrian mafic and felsic volcanic rocks, interstratified with sedimentary rocks, outcrops there. The results allow us to reconstruct the local paleogeographic and structural environment, which prevailed during and between the successive igneous episodes and also allow for an assesment of the deformation of the continental lithosphere during the whole period.

2. Geological setting

The studied area is located in the Iberian Massif, in the central part of the Ossa-Morena Zone (OMZ) (Fig. 1). Polyphase ductile deformation and metamorphism in the Ossa-Morena Zone are related to a complex evolution including two major tectonothermal episodes of Cadomian (late Proterozoic to early Cambrian) and Variscan age (Middle to Late Paleozoic). Deformation was controlled strongly by the existence of a Cadomian basement and a Paleozoic sedimentary cover. Both the basement and the cover were involved in Variscan tectonics, resulting in large-scale strain partitioning. In the basement important ductile to brittle–ductile shear zones developed, whereas the sedimentary cover was affected by large fold nappes with axial-planar cleavage and brittle-ductile low-angle thrusts. At scale of the Variscan chain, the OMZ correlates with the northern margin of the Armorican Zone and the southern part of the Saxothuringian Zone and/or Tepla-Barrandian Zone of the Bohemian Massif (Eguíluz et al., 1995, 2000; Franke et al., 1995; Murphy et al., 2002).

Volcano-sedimentary formations crop out on both flanks of the Monesterio Antiform. They formed between 520 and 500 Ma (Middle to late Cambrian; Nägler, 1990; Ochsner, 1993; Ordóñez, 1998), and were only slightly affected by Variscan events. Traditionally, they have been subdivided into several fault-bounded troughs (called *cubetas*) showing important stratigraphic and paleontological differences from one to another (Liñán, 1984; Liñán et al., 1997). Nevertheless, Eguíluz et al. (1997, 2000) have demonstrated the lateral continuity between some of these troughs, suggesting that during Cambrian times only one basin, with lithological and thickness variations, existed. From a stratigraphic point of view, there is a general agreement on the division of the OMZ Cambrian sequence in three successive

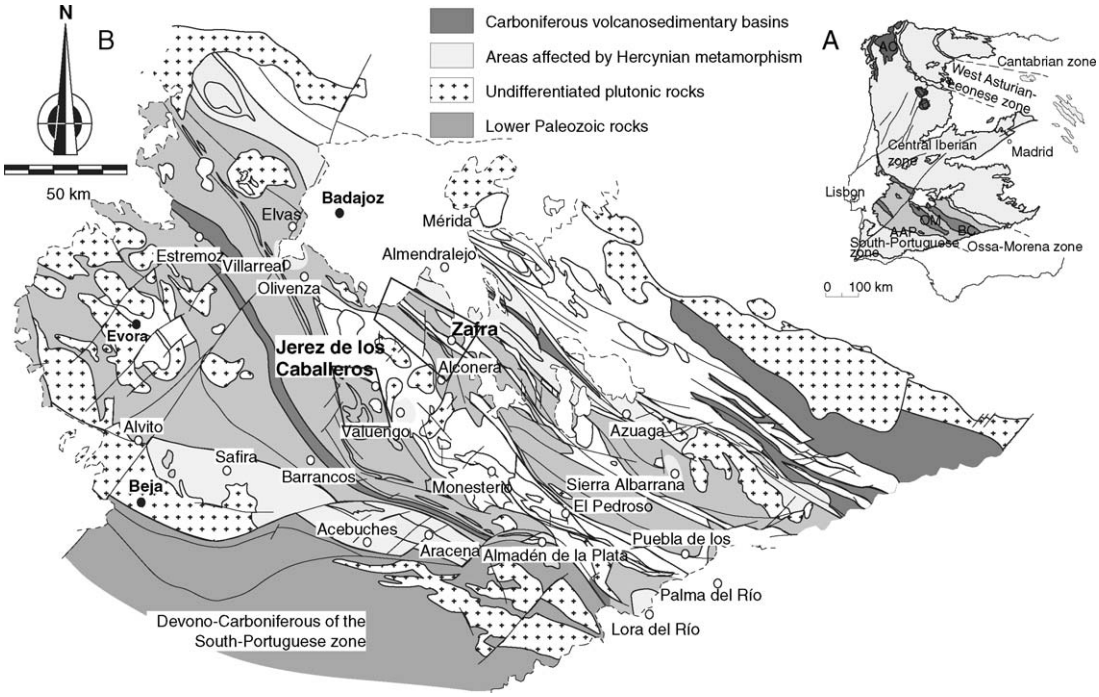

Fig. 1. (A) Geological sketch of the Iberian Massif showing the main zones; AC, Allochthonous complexes; BC, Badajoz-Córdoba shear-zone; OM, Olivenza-Monesterio Antiform; AAP, Aracena-Almadén de la Plata belt. (B) Simplified geological map of the Ossa-Morena Zone. Specific study areas are in sectors of Zafra (north flank; Figs. 3 and 5) and Jerez de los Caballeros (south flank; Fig. 4).

sedimentary formations (Fig. 2): Lower Detritic, Intermediate Carbonate and Upper Detritic.

The structure of both flanks is simple. The northern flank displays a synclinal-anticlinal structure bounded to the north by a N120°E trending vertical fault (Fig. 3). The southern flank also shows a synclinal-anticlinal structure truncated by a reverse fault by which the Upper Detritic Formation is thrust over the Intermediate Carbonate (Fig. 4). All lithologies show a low-grade metamorphism that increases southwards up to greenschist facies conditions.

On the northern flank, in the Zafra-Nogales sector (Fig. 3), the Lower Detritic Formation unconformably overlies the Malcocinado Fm which consists of Late Neoproterozoic to earliest Paleozoic volcanosedimentary deposits (Liñán, 1978; Liñán et al., 1984; Quesada et al., 1990). It includes a basal continental conglomerate (Liñán, 1978) passing upward to transitional arkoses and finally to marine shales with ripple and flute structures. Basal conglomerates and arkoses, deposited in fluvial and deltaic environments, are interpreted to reflect formation of a relief with its related hydrographic network. The upper part of the Lower Detritic Formation formed on a very shallow marine shelf (Liñán and Fernández-Carrasco, 1984) and documents an increase of the subsidence of the sedimentary basin. The overlying Intermediate Carbonate Formation was related to the maximum of the marine transgression (Liñán and Quesada, 1990). Mainly clastic, it was deposited on a storm-dominated platform (Liñán and Gámez-Vintáned, 1993). Locally, massive and thick limestones with archeocyathids occur (Roso de Luna and Hernández-Pacheco, 1955; Perejón and Moreno-Eiris, 1992). The Upper Detritic Formation consists of very fossiliferous brown-greenish shales deposited in an open shelf, with increasing sandy components upwards and some thick sandstone subunits such as the Castellar Quartzite. The thickness (up to 40 m) and composition of this shallow marine quartzite subunit varies laterally, disappearing in some places and changing from quartz-arenite to a finer alternation of thin sandstones and shales. This quartzite horizon, which formed at the Lower–Middle Cambrian boundary (Fig. 2), is correlated with the Hawke Bay worldwide regression (Palmer and James, 1980; Liñán et al., 1997). The pelitic-sandy sequence overlying this quartzite has been interpreted to reflect an important deepening of the basin (Sánchez García et al., 2003). However, this interpretation does not agree with the subaerial or very shallow submarine conditions of synchronous eruptions (Etxebarria, 2003; Etxebarria et al., 2004). The volcanic activity began just before the sed-

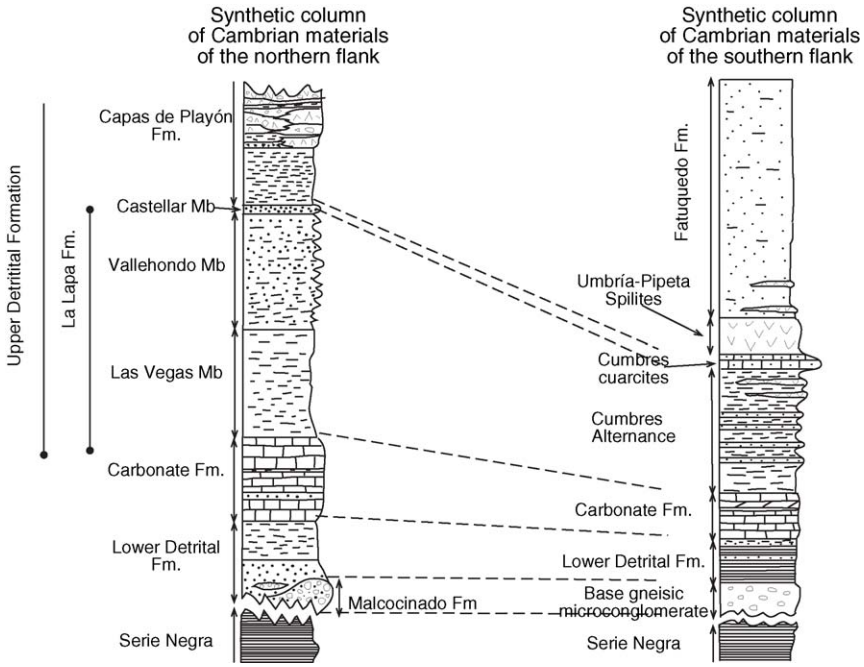

Fig. 2. Synthetic stratigraphy of the Cambrian series of the northern and southern flanks, Monesterio Antiform.

imentation of the Castellar Quartzite (520 ± 17 Ma, Sm–Nd whole rock; Nägler, 1990), thus only in the upper part of the Upper Detritic Formation (Fig. 5). The eruptions would have stopped during the Middle Cambrian (based on acritarchs in the youngest sediments, (Palacios, personal communication, 2005) and radiometric dates (515 ± 35 Ma, Sm–Nd whole rock; Nägler, 1990).

On the southern flank, in the Jerez de los Caballeros sector (Fig. 4), the Lower Detritic Formation unconformably overlies a pre-tectonic conglomerate with a laminated ignimbritic matrix similar to that of the Malcocinado Fm occurring in the northern flank (Fig. 2), which itself unconformably overlies Late Proterozoic rocks (Muelas et al., 1977). Locally the Lower Detritic Formation conformably overlies Proterozoic rocks of the Monesterio Antiform core. This Lower Detritic Formation consists mainly of arkoses, graywackes and shales with some interstratified volcanic deposits. It progressively passes to clastic limestones of the Intermediate Carbonate Formation. The Upper Detritic Formation consists of four units from base to top (Fig. 2): (1) alternation of mudstone, sandstone and lava flows; (2) sandy horizon (quartzite); (3) alternation of lava-flows, tuffs, tuffites and tuffaceous deposits; (4) argillaceous and sandy deposits. With the possible exception of the first coarse-grained clastic deposits at the base of the Lower Detritic Formation, which could be fluvial, all the sediments are shallow marine and recorded a more or less active subsidence of the basin.

3. Succession of volcanic events

On the northern flank, the eruptive dynamics were mainly explosive and lava flows are rare, reflecting the predominance of felsic products over mafic ones. Four volcanic episodes can be distinguished on the northern flank (Fig. 5). The first episode predates the Castellar Quartzite, and consists of rhyolitic lava flows in the western area, with trachyandesitic lava flows and volcanoclastic materials to the east. These initial volcanic deposits are interstratified with mudstones and sandstones. The second episode postdates the Castellar Quartzite. It corresponds to lava flows and pyroclastic-fall and -flow deposits which have a trachy-andesitic to trachytic composition. Interstratified sedimentary deposits, rare in the western area, are more voluminous in the eastern one. There, sandy sediments alternate with lava flows and a few pyroclastic deposits. Lava sills with the same composition as the eruptive products are also intrusive within this sequence. The third episode is recorded only in the western area. It corresponds to rhyolitic, trachytic and trachyandesitic lava flows and pyroclastic deposits, alternating with reworked volcanic deposits and shales. The fourth and last volcanic episode is mainly composed of trachy-andesitic lava flows, some-

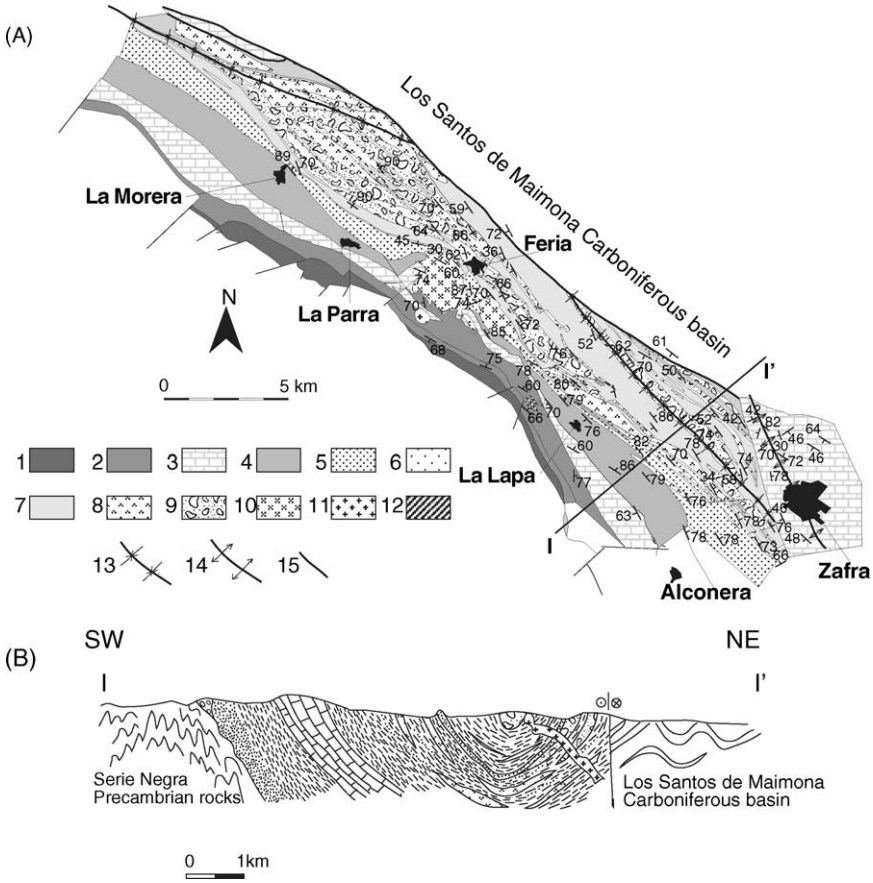

Fig. 3. (A) Geological map of the northern flank (Zafra-Nogales area). (B) Cross-section on the I–I′ line (location on A). 1, Malcocinado Fm.; 2, Lower Detritic Fm.; 3, Intermediate Carbonate Fm.; 4, Las Vegas member; 5, Vallehondo member; 6, Castellar member; 7, Capas de Playón Fm.; 8, Lava flows and sills; 9, Volcaniclastic rocks; 10, Granitic intrusions; 11, Gabbros; 12, Dykes and necks; 13, Syncline; 14, Anticline; 15, Faults.

times pillowed, and pyroclastic flow and fall tuffs of the same composition.

Two volcanic episodes can be identified on the southern flank despite the greenschist metamorphism that somewhat obliterates the original volcanic textures. The first one is represented by a few volcanic materials interstratified within the Lower Detritic Formation, suggesting that volcanic activity started much earlier than on the northern flank. The second episode corresponds to large volumes of volcanics within the Upper Detritic Formation. The eruptive activity was mainly extrusive (lava flows or even pillows) and shallow marine, and mafic products predominate over felsic ones. The pillow lavas form thick layers interstratified with lava flows, both being interstratified within shallow marine sediments. Pyroclastic events are rare, as expected for submarine eruptions.

On both flanks, small bodies of gabbro, diorite, granite and albitite (alkali feldspar microsyenites) are found as intrusions within the Cambrian sequence. Their shape is irregular or tabular in the southern flank, suggesting a possible intrusive process as sills and dykes; on the northern flank the intrusives are rounded and much less abundant. Gabbros and diorites have diabasic to ophitic textures in thin section whereas albitites and granites are granular. The intrusives mainly crosscut the Intermediate Carbonate Formation, sometimes the Lower Detritic Formation and although they may cut the Upper Detritic Formation, they are typically associated with volcanics. Albitites and granites crosscut the Upper Detritic Formation, and albitites sometimes crosscut the gabbros. The albitites present a holocrystalline phaneritic texture formed from $\mathrm{Alb} + \mathrm{Qtz} + \mathrm{Kfs} \pm \mathrm{Am}$. The samples with amphibole usually show opaques, epidote and sphene. Based on their compositions, the intrusive rocks originated from the same mantle and crustal sources as the volcanics. They were probably emplaced just after or even during the end of the volcanic activity.

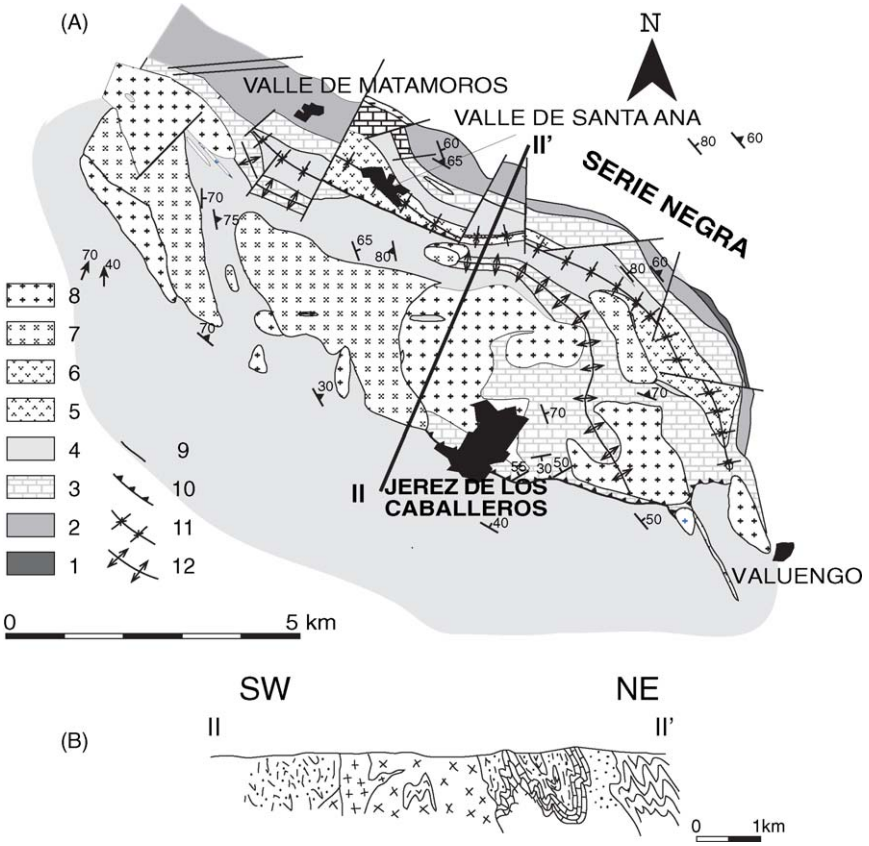

Fig. 4. (A) Geological mapping of the southern flank (Jerez de los Caballeros area). (B) Cross-section on the I–I′ line (location on A). 1, Strongly deformed conglomerate; 2, Lower Detritic Fm.; 3, Intermediate Carbonate Fm.; 4, Upper Detritic Fm.; 5, Felsic lava flows; 6, Mafic lava flows and sills; 7, Albitites; 8, Gabbros; 9, Vertical faults; 10, Reverse faults; 11, Syncline; 12, Anticline.

4. Dynamics of eruptions and influence on the sedimentation

Field and petrographic observations enable us to identify a great variety of extrusive products (Fig. 6A), including pyroclastic products, lava flows, lava domes and shallow sills. Monolithologic tuffs are interpreted as flow breccias associated with lava flows. Their compositions are basaltic to rhyolitic and textures are porphyritic, microlitic, trachytic or intersertal and mostly vessiculated. Devitrification textures (spherulitic and/or micro- to crypto-granular) are common in the groundmass (Fig. 6B). Mafic lavas frequently show quenched textures in their interstitial matrix, as is usual for submarine lavas.

The pyroclastic products mainly originate from nuées ardentes eruptions. The pyroclastic flow, surge and fall deposits may be rhyolitic, dacitic, trachytic and trachyandesitic. Sedimentary reworking of volcanic materials is common, and in some cases can be interpreted as turbiditic deposits. Their general features can be summarized as follows.

The *pyroclastic flow deposits* show a massive internal structure, without any stratification. They are poorly sorted (0.1–50 mm), with a clast- or matrix-supported fabric. Locally, they show a chaotic flow foliation, flow folds or eutaxitic texture typical of welded ignimbritic facies. Pumice fragments and phenocrysts fragments are scattered within a vitroclastic matrix, together with cognate juvenile clasts and minor xenoliths of various origins. Pumice and scoria fragments may be plastically deformed, flattened and welded, and adopt the shape of fiammes. They can include skeletic or dendritic phenocrysts or microlites (Fig. 6C). The matrix and cement amount is variable (10–40 vol.%). Glass-shards show different forms depending on glass composition: trachyandesitic shards are mostly scoriaceous or blocky. Trachytic and rhyolitic ones are mainly platy, cuspate, Y shaped or pumiceous (Etxebarria, 2003).

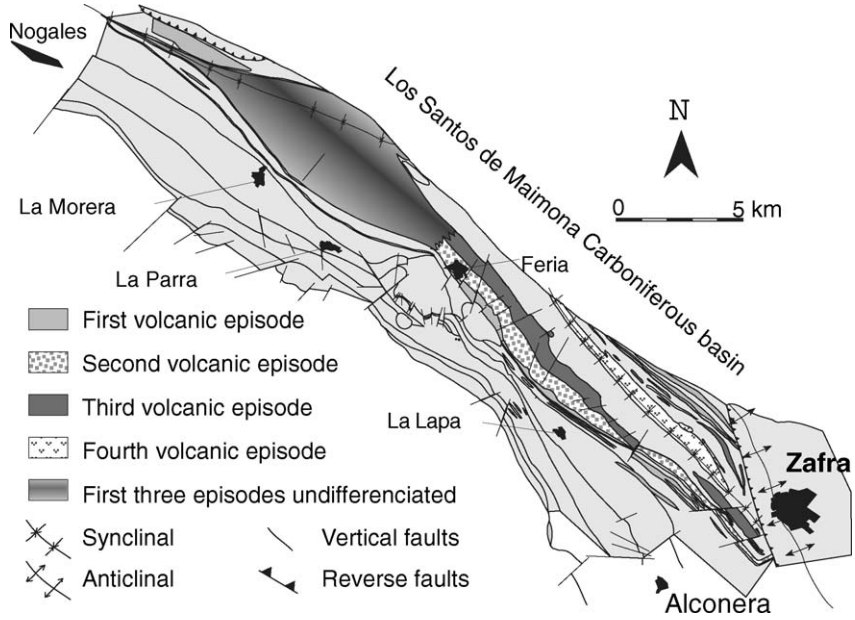

Fig. 5. Volcanic episodes on the northern flank (Zafra-Nogales area).

The most abundant non-vesicular clasts, with a trachytic, granular or microgranular texture, have a composition similar to that of glass fragments. They are cognate juvenile clasts, likely produced by the fragmentation of the inner wall of the magmatic reservoir. Xenoliths show a composition very different from that of glassy clasts. They likely formed by fragmentation of the country rocks during eruptions. The pyroclastic

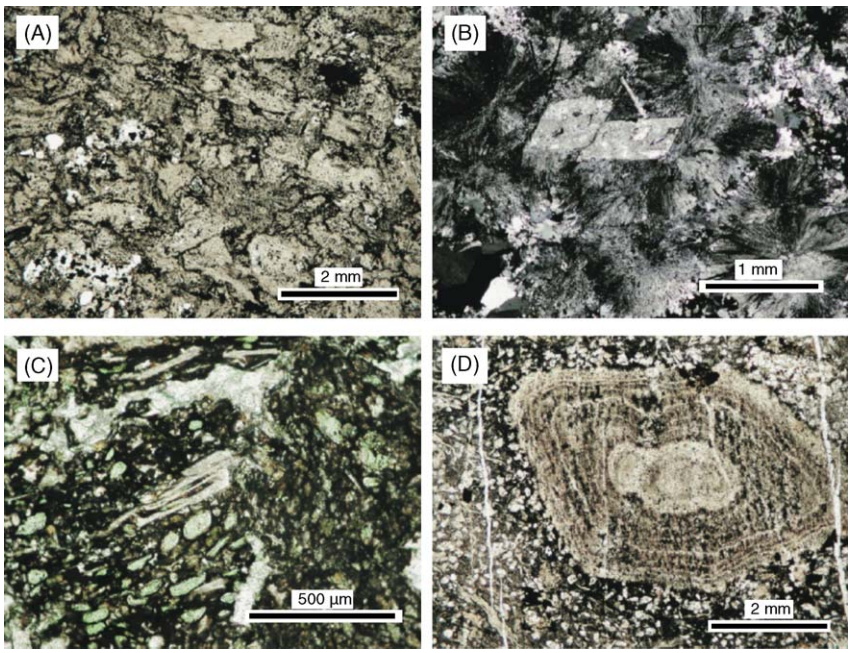

Fig. 6. (A) Adaptation of glassy fragments in a surge or fall deposit; (B) devitrification textures in rhyolitic sills; (C) skeletal textures in a trachyandesitic pyroclastic flow deposit; (D) accretionary lapilli in a surge or fall deposit.

flow deposits, within which these xenoliths predominate among juvenile clasts, could be the earliest products from phreatomagmatic eruptions.

On the southern flank, the pyroclastic flow deposits show a more intense tectonic deformation (Fig. 7A) and could correspond to the main and central unit of a nuée ardente (Sparks et al., 1973). The absence of welded tuffs and the scarcity of pyroclastic deposits, contrasting with the abundance of lava flows and pillow lavas supports the hypothesis that the explosions occurred in shallow marine conditions.

The *surge or fall deposits* are found only on the northern flank. They correspond to thin laminated horizons (<up to 50 cm in thickness), which may be poorly (0.1–10 mm) or quite well sorted (0.1–1 mm) with sometimes a coarse normal graded bedding. They may be clast- or matrix-supported. Those with poor sorting are mainly formed by a vitroclastic matrix including flattened, compacted and slightly welded glassy lapilli and ash fragments, phenocrysts and phenocrysts fragments (10–20%) and lithic cognates. Occasionally they include some cm-thick layers of accretionary lapillis (Fig. 6D). The well sorted ones are formed by blocky or X and Y shaped glass-shards and phenocrysts fragments and phenocrysts in an abundant vitroclastic matrix. They form 10 cm-thick beds horizontally or cross-laminated (Fig. 7B). Always associated with pyroclastic flow deposits, they may be interpreted either as subaerial air fall or surge deposits. Traction structures have been found only in the cross laminated well sorted ashes, which would most probably represent surge deposits. Nevertheless, most of these horizontally bedded or laminated deposits may be fall out deposits, or formed by gravitational collapse of vertical eruptive columns. The coarsest laminated facies would represent the most proximal deposits to the source and finest massif ones the most distal ones.

The *ground surge deposits* correspond to massive and never stratified 10 cm-thick strata. They are phenocrysts fragment rich (up to 50% in volume), very poorly sorted (0.1–50 mm) and clast- to matrix-supported. Clasts are often plastically deformed and locally welded. Flow foliation may be common. This crystal-rich deposit may have formed by sedimentation of the heaviest particles at the bottom or the front of pyroclastic flows (Sparks et al., 1973). They could also represent crystal-enriched deposits formed by suspension of the lightest particles within the cloud overlying the pyroclastic flow (McPhie et al., 1993).

The *lag-breccia deposits* form massive m-thick horizons. They are clast-supported and very poorly sorted. They include coarse lapilli fragments (2–60 mm) within an ashy matrix. They may represent *lag-breccia* or *proximal coarse lithic breccia* deposits (Druitt and Sparks, 1982), formed near the vent as a result of the early and

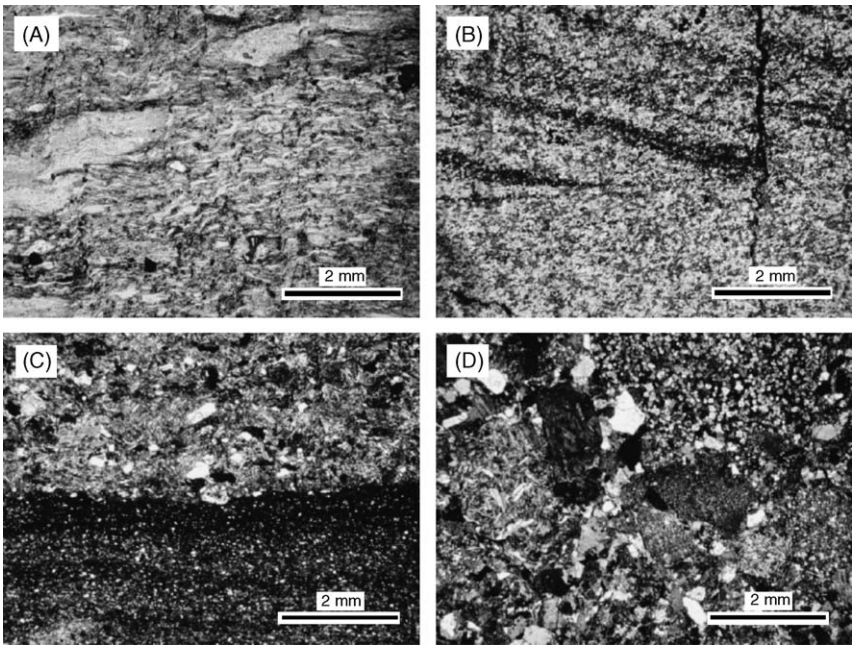

Fig. 7. (A) Foliated pyroclastic tuff from the southern flank; (B) cross-laminated ash cloud surge deposit; (C) contact metamorphosed surface of a sedimentary deposit caused by a surge deposit; (D) tuffite showing its large variety of clasts.

fast deposition of the densest and coarsest components of the pyroclastic flow.

All these pyroclastic materials originate from explosions with a very high capacity of fragmentation and dispersion. The frequent welding and ductile adaptation of glassy clasts (Fig. 6A), and the "thermally cooked surfaces" (Fig. 7C) of underlying sediments indicate that the deposition occurred at high temperature in subaerial or very shallow subaqueous conditions. In any case, the accretionary lapilli attest to subaerial eruptions. Moreover, some m-thick levels of pyroclastic breccia (lag-breccia or proximal coarse lithic breccia; Druitt and Sparks, 1982) with a very limited lateral extent in the western area of the northern flank indicate the proximity of an eruptive center.

The *tufaceous deposits* include submarine pyroclastic flow and fall deposits, as well as deposits formed by the remobilization of non-consolidated pyroclastic products in a shallow subaqueous environment (Fig. 7D). The volcanic pumice clasts are more or less rounded. Sedimentary monocrystalline quartz grains are very abundant (10–30%) and a carbonate or volcanic cement may occur.

Other volcaniclastic facies have also been identified, such as turbiditic deposits formed by rounded volcanic fragments, normal graded forming 10 cm-thick beds interstratified with lava flows and pyroclastic flows.

5. Local paleogeographic evolution during the Cambrian period

The Cambrian paleogeography corresponds to a rifting structure on the margin of a marine basin, as demonstrated by the development of different basins with their own stratigraphic and paleontological characteristics (Liñán and Perejón, 1981; Liñán and Quesada, 1990; Sánchez García et al., 2003), or that of a unique general sedimentary basin consisting of interconnected small sub-basins (Giese and Bühn, 1993; Eguíluz et al., 1997, 2000). In any case, the conditions within which volcanic processes happened are equivalent. As the lower Cambrian detritic sediments are coarser towards the north of the OMZ, the coastline of the basin was located somewhere on the northern flank of the Monesterio Antiform.

On the northern flank, the sedimentary features and the fossil content of Cambrian sediments (Liñán and Gámez-Vintáned, 1993) indicate that the deposition began in subaerial to littoral environments (Torreárboles Fm.), and continued in a more widespread and open shallow marine environment on a variably subsiding basement. The regressive period, which took place between the two main transgressive periods, culminated with the uppermost sandy formation deposit of the Upper Detritic Formation (Castellar Quartzite; Liñán et al., 1997). In such a context, accounting for the subaerial feature of eruptions and most of the volcanic accumulations, the successive volcanic periods were synchronous with emersions probably generated by the buildup of volcanic edifices. On the southern flank, the eruptions took place in a permanently submarine and deeper basin, the subsidence of which changed with time.

In detail, the eastern area (between Zafra and La Lapa) on the northern flank displays a higher sediment/volcanics ratio (ca. 1) than the western area (<1) for the first three volcanic episodes (Fig. 3). This ratio likely indicates that the eruptive centers were particularly abundant on the western area, an inference also supported by the large quantity of proximal pyroclastic materials there.

These pieces of evidence suggest the building of a stratovolcano with vulcanian, plinian or subplinian activities from the first to the third volcanic episode in the western area of the northern flank (Fig. 8). These episodes were synchronous with ephemeral emersions of the sediments. During the successive and much longer periods of volcanic inactivity, the basement subsided. The mafic eruptions of the fourth episode suggest the existence of several shield type volcanic edifices (Fig. 9). Each of them had a large lateral extension, gentle slopes and was partially submerged at its periphery, as typical island basaltic volcanoes.

On the southern flank, the materials are not enough well preserved to reconstruct in detail the Cambrian environments, but the eruptions were clearly submarine. Lava flows are most common, but explosions sometimes occurred. There are neither particular accumulation of volcanic material on some sites, nor volcanic breccias indicative of the proximity of the vents. The eruptions were fissural, and not centered as on the northern flank.

6. Major element geochemistry of volcanics; possible involved mantle and crustal sources

The analyzed samples (Table 1) are representative of the main lithologies of Cambrian extrusive and intrusive magmatic rocks outcropping from base to top within both flanks of the Monesterio Antiform. One hundred and thirty whole rock samples were analysed for major elements at the Oviedo University with a Phillips PW2404 fluorescence X spectrometer. The error accepted for major element data is always lower than 1% (Ariño, personal communication, 2005).

The loss on ignition (LOI), due to secondary alteration effects on these Cambrian rocks, may be rather significant (from 0.5 to 4% on an average; up to 12%).

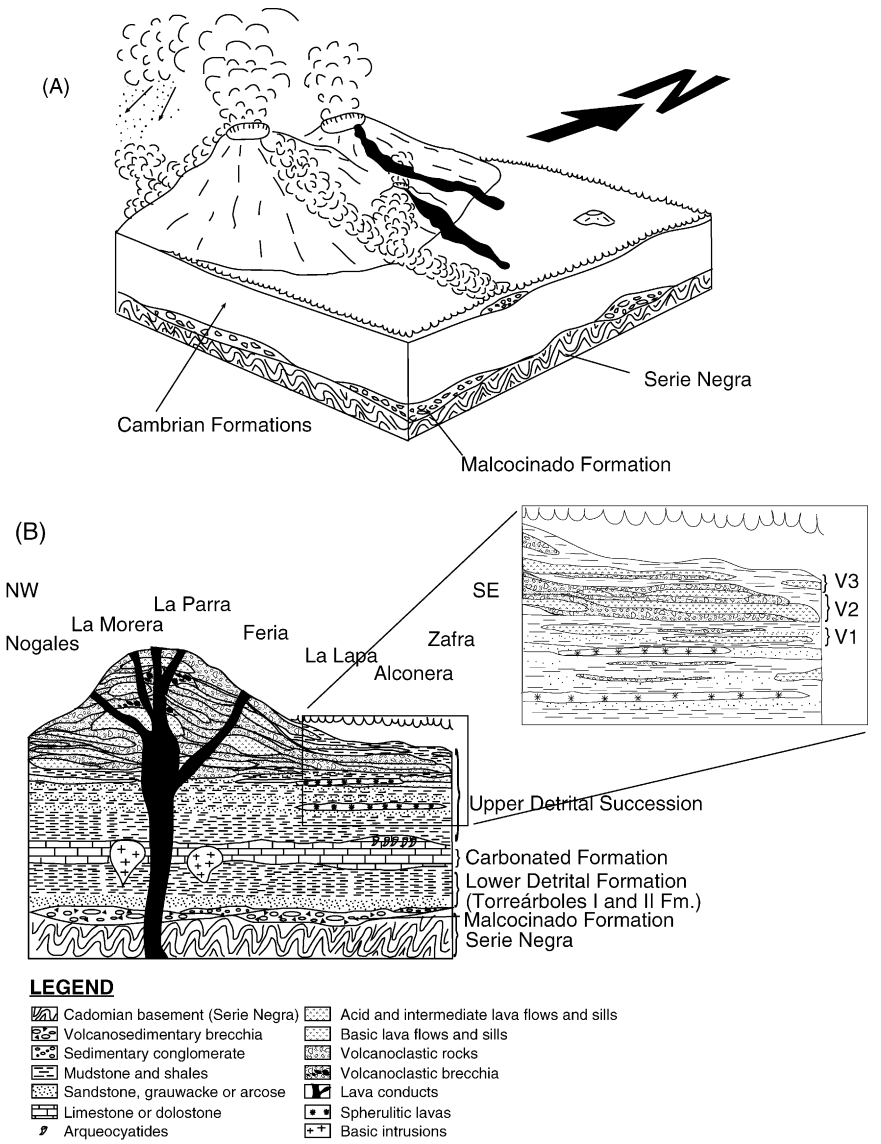

Fig. 8. (A) Paleogeographic setting for the first three magmatic episodes; (B) related cross-section.

This LOI is not correlated with a systematic loss or gain in alkali and silica (Fig. 10). A number of samples with rather high or low K_2O or Na_2O contents have a very low LOI, which suggests that these contents may be primary. Only the samples with extremely high LOI (above 6%) likely suffered a loss of SiO_2. In order to keep to a minimum alteration effects, the study of major element compositions was done on the compositions recalculated on a volatile free basis (Tables 1–3).

When the total alkali is plotted against SiO_2 (Fig. 11), magmatic rocks from both flanks form a large set from mafic (down to 43% SiO_2) to felsic (up to 82% SiO_2) compositions mostly, but not exclusively, within the sub-alkaline field (Le Maitre, 1989). The total of alkali ranges from 2 to 7% for mafic rocks, and from 4 to 12% for the felsic rocks. On the whole, extrusive and intrusive rocks from both flanks of the antiform do not form separate groups.

In detail, the mafic rocks are somewhat diversified. Some from the N flank plot within the alkali-rich (3–7%) and silica under-saturated field. Conversely, those from the S flank plot within the alkali poor (2–3%) and silica oversaturated field; they display a sub-alkaline and tholeiitic affinity.

All the intrusive felsic rocks, including albitites, plot within the granite field with a sub-alkaline affinity. Nev-

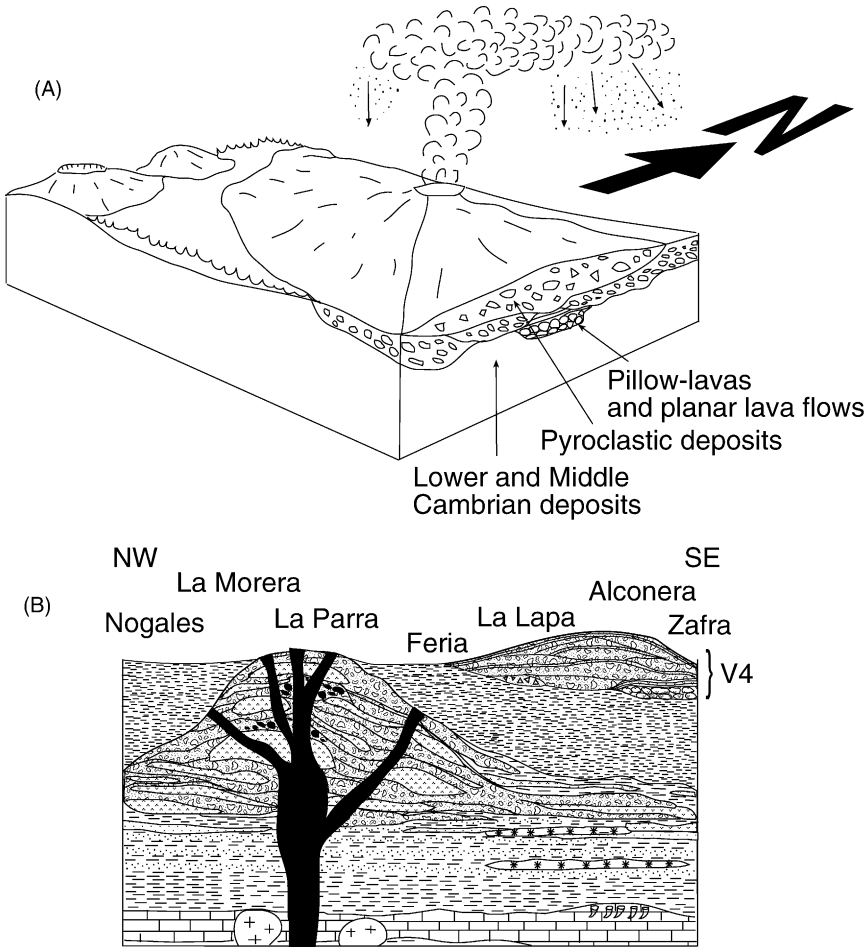

Fig. 9. (A) Paleogeographic setting for the fourth magmatic episode; (B) related cross-section.

ertheless three groups exist (Feria granites; Sierra Vieja granites; S flank albitites), each of them having a rather limited compositional range compared to those of felsic volcanics. As for the mafic intrusives, the granites from the N flank are richer in alkali and also in silica than those from the S flank.

In the Harker diagrams (Fig. 12A and B), data from each flank are presented separately. Both data sets do not form a continuous series, and display a bimodal distribution with two well developed end-members, mafic and felsic, and a third intermediate small group.

The most mafic rocks from both flanks can be representative of rather primitive mantle liquids with up to 13.5% MgO, 16% Fe_2O_{3T}, 11% CaO in the volcanics and 14% CaO in the intrusives. These liquids were also alkali-rich (up to 5% Na_2O; up to 2% K_2O). However, the mafic rocks from the N flank are significantly richer in TiO_2 (up to 5%) and P_2O_5 (up to 1.5%), as usual for silica-undersaturated rocks (Wilson, 1989). On the S flank, the gabbros are much poorer in Na_2O, K_2O and P_2O_5 than basalts.

Within the mafic group of each flank, SiO_2 correlates roughly negatively, as usual, with MgO, CaO, Fe_2O_3, Al_2O_3, TiO_2 and P_2O_5. Nevertheless, SiO_2 correlates negatively with Na_2O and K_2O in the N flank, but positively in the S flank.

This inverse correlation between silica and alkali in the N flank could trace mantle partial melting relationships where the highest alkali contents and the lowest silica contents in the melt correspond to the lowest melting degree. Melting of metasomatic silica-poor mantle minerals such as pargasite and Na-rich diopside would be mainly responsible for these variations. The positive correlations between alkalis, TiO_2 and Fe_2O_{3T} also support this hypothesis. This type of metasomatized mantle source is similar to what is described for the lithospheric continental mantle (Chalot-Prat and Boullier, 1997; Pecerillo, 1999; Pecerillo and Panza, 1999; Chalot-

Table 1
Representative major element analysis of Cambrian igneous rocks from the northern flank of the Monesterio Antiform

Rock name	Tephrite	Gabbro	Tephrite	Picrobasalt	Gabbro	Gabbro	Gabbro	Gabbro	Trachyandesite	Gabbro	Trachyandesite	Trachyte/ trachydacite	Trachyandesite	Trachyandesite	Trachyte/ trachydacite	Trachyte/ trachydacite
Sample	EFE-22	EG-FL-1	ESF-2	EG-BA-1	EG-GA-3	EG-GA-1	EG-GA-2	EG-TO-3	EFE-12	EG-AL-1	EAC-8	EG-LM-3	EAC-1	EG-ER-1	ELP-2	EG-LM-6
SiO_2	41.25	42.07	42.2	42.41	45.37	46.36	47.9	51.44	53.48	58.04	59.13	59.28	59.6	61.47	63.16	63.81
TiO_2	2.85	4.79	3.12	2.82	4.69	1.94	3.00	2.04	4.17	0.91	1.72	0.75	0.88	1.11	0.95	0.50
Al_2O_3	17.48	12.31	13.9	13.21	12.94	14.58	14.89	13.89	22.25	16.15	15.81	18.27	14.35	14.74	16.66	13.52
Fe_2O_3t	11.96	16.62	13.9	13.31	16.35	11.34	11.62	13.21	2.23	7.13	10.11	5.77	6.45	9.42	5.85	6.71
MgO	2.37	5.13	4.21	5.19	5.17	7.74	6.66	4.92	0.36	3.93	0.29	0.55	0.89	1.93	0.23	0.65
CaO	8.42	9.01	7.44	8.35	7.67	11.35	9.39	6.06	2.18	3.71	0.90	1.18	3.70	0.73	0.32	0.73
MnO	0.15	0.25	0.18	0.16	0.27	0.20	0.18	0.22	0	0.11	0.10	0.08	0.18	0.03	0.12	0.21
Na_2O	4.56	3.71	2.77	2.51	3.55	2.20	2.65	4.79	5.32	4.82	5.21	4.94	3.40	4.08	5.25	5.04
K_2O	1.84	0.91	0.63	0.23	1.17	1.07	1.55	0.67	4.3	1.54	3.79	6.97	4.31	3.22	4.55	4.47
P_2O_5	0.91	1.23	0.49	0.42	0.65	0.30	0.25	0.25	1.94	0.20	0.64	0.24	0.23	0.33	0.21	0.07
LOI	8.40	3.99	11.23	11.48	2.03	2.63	1.83	2.32	3.01	3.07	1.58	2.01	5.83	2.44	1.97	4.16
Total	100.19	100.02	100.07	100.09	99.86	99.72	99.92	99.80	99.24	99.60	99.28	100.04	99.82	99.49	99.27	99.87
Percent oxides recalculated on a volatile-free basis																
SiO_2	44.94	43.81	47.50	47.86	46.38	47.75	48.83	52.77	55.58	60.13	60.52	60.47	63.41	63.34	64.91	66.67
TiO_2	3.10	4.99	3.51	3.18	4.79	2.00	3.06	2.09	4.33	0.94	1.76	0.77	0.94	1.14	0.98	0.52
Al_2O_3	19.04	12.82	15.65	14.91	13.23	15.02	15.18	14.25	23.12	16.73	16.18	18.64	15.27	15.19	17.12	14.13
Fe_2O_3t	13.03	17.31	15.65	15.02	16.71	11.68	11.85	13.55	2.32	7.39	10.35	5.89	6.86	9.71	6.01	7.01
MgO	2.58	5.34	4.74	5.86	5.28	7.97	6.79	5.05	0.37	4.07	0.30	0.56	0.95	1.99	0.24	0.68
CaO	9.17	9.38	8.37	9.42	7.84	11.69	9.57	6.22	2.27	3.84	0.92	1.20	3.94	0.75	0.33	0.76
MnO	0.16	0.26	0.20	0.18	0.28	0.21	0.18	0.23	0.00	0.11	0.10	0.08	0.19	0.03	0.12	0.22
Na_2O	4.97	3.86	3.12	2.83	3.63	2.27	2.70	4.91	5.53	4.99	5.33	5.04	3.62	4.20	5.40	5.27
K_2O	2.00	0.95	0.71	0.26	1.20	1.10	1.58	0.69	4.47	1.60	3.88	7.11	4.59	3.32	4.68	4.67
P_2O_5	0.99	1.28	0.55	0.47	0.66	0.31	0.25	0.26	2.02	0.21	0.66	0.24	0.24	0.34	0.22	0.07
Total	100	100	100	100	100	100	100	100	100	100	100	100	100	100	100	100

Rock name	Dacite	Trachyte/ trachydacite	Trachyte/ trachydacite	Trachyte/ trachydacite	Granite	Rhyolite	Granite	Dacite	Granite	Rhyolite	dacite	Rhyolite	Dacite	Granite	Rhyolite	Rhyolite
Sample	EG-LM-4	EFE-31	ESF-3	EG-TR-1	EG-F-5	E-5	EG-F-2	E-8	EG-F-1	EG-LM-1	EG-ES-1	EGT-1	EM-1-2	F-1	EFE	EG-CA-1
SiO_2	66.22	66.35	68.14	68.77	69.75	69.93	69.95	70.1	70.47	70.51	70.79	71.28	71.69	71.84	72.18	72.34
TiO_2	0.66	0.97	0.54	0.22	0.63	0.53	0.55	0.43	0.57	0.31	0.33	0.53	0.46	0.27	0.27	0.35
Al_2O_3	11.98	15.68	14.98	13.92	11.39	9.96	14.17	8.47	14.1	15.09	7.99	13.39	9.78	13.77	14.43	9.31
Fe_2O_3t	8.04	4.67	3.29	3.98	8.06	10.36	4.70	9.00	3.74	2.06	7.44	4.95	10.08	0.96	0.35	6.55
MgO	0.39	0.12	0.23	0.09	0.06	0.03	0.41	0.91	0.09	0.57	0.89	0.04	0.08	0.15	0.10	0.43
CaO	1.98	0.18	0.03	0.97	0.08	0.07	0.27	0.98	0.40	1.14	0.94	0.15	0.05	0.03	0.05	0.17
MnO	0.12	0.01	0	0.11	0.02	0.13	0.02	0.12	0.08	0.03	0.36	0.08	0.01	0	0	0.26
Na_2O	2.53	5.66	0.91	5.79	3.86	3.08	7.61	2.32	8.41	3.80	2.23	7.55	2.29	0.25	0.76	2.49
K_2O	4.90	4.75	9.15	3.89	4.02	4.29	0.72	3.92	0.13	4.10	2.80	0.11	2.97	10.47	9.99	3.75
P_2O_5	0.07	0.08	0.04	0.04	0.03	0.03	0.12	0.01	0.13	0.12	0.02	0.09	0.03	0.03	0.03	0.01
LOI	2.44	0.85	1.90	1.60	1.18	0.86	0.75	3.15	0.92	2.26	5.64	0.93	1.67	1.38	0.95	3.48
Total	99.33	99.32	99.21	99.37	99.06	99.27	99.28	99.41	99.02	99.99	99.43	99.10	99.11	99.15	99.11	99.15

Table 1 (*Continued*)

Rock name	Dacite	Trachyte/ trachydacite	Trachyte/ trachydacite	Trachyte/ trachydacite	Granite	Rhyolite	Granite	Dacite	Granite	Rhyolite	dacite	Rhyolite	Dacite	Granite	Rhyolite	Rhyolite
Sample	EG-LM-4	EFE-31	ESF-3	EG-TR-1	EG-F-5	E-5	EG-F-2	E-8	EG-F-1	EG-LM-1	EG-ES-1	EGT-1	EM-1-2	F-1	EFE	EG-CA-1
Percent oxides recalculated on a volatile-free basis																
SiO_2	68.35	67.38	70.02	70.34	71.26	71.06	70.99	72.82	71.83	72.15	75.48	72.61	73.57	73.48	73.53	75.61
TiO_2	0.68	0.99	0.55	0.23	0.64	0.54	0.56	0.45	0.58	0.32	0.35	0.54	0.47	0.28	0.28	0.37
Al_2O_3	12.36	15.92	15.39	14.24	11.64	10.12	14.38	8.80	14.37	15.44	8.52	13.64	10.04	14.08	14.70	9.73
Fe_2O_3t	8.30	4.74	3.38	4.07	8.23	10.53	4.77	9.35	3.81	2.11	7.93	5.04	10.34	0.98	0.36	6.85
MgO	0.40	0.12	0.24	0.09	0.06	0.03	0.42	0.95	0.09	0.58	0.95	0.04	0.08	0.15	0.10	0.45
CaO	2.04	0.18	0.03	0.99	0.08	0.07	0.27	1.02	0.41	1.17	1.00	0.15	0.05	0.03	0.05	0.18
MnO	0.12	0.01	0.00	0.11	0.02	0.13	0.02	0.12	0.08	0.03	0.38	0.08	0.01	0.00	0.00	0.27
Na_2O	2.61	5.75	0.94	5.92	3.94	3.13	7.72	2.41	8.57	3.89	2.38	7.69	2.35	0.26	0.77	2.60
K_2O	5.06	4.82	9.40	3.98	4.11	4.36	0.73	4.07	0.13	4.20	2.99	0.11	3.05	10.71	10.18	3.92
P_2O_5	0.07	0.12	0.04	0.04	0.03	0.03	0.12	0.01	0.13	0.12	0.02	0.09	0.03	0.03	0.03	0.01
Total	100	100	100	100	100	100	100	100	100	100	100	100	100	100	100	100

Rock name	Rhyolite	Dacite	Granite	Granite	Granite	Rhyolite	Granite	Rhyolite	Granite	Granite	Granite	Rhyolite	Rhyolite	Rhyolite
Sample	E-7	E-9	F-3	EG-SV-1	EG-SV-3	EAL-6	EG-SV-2	EG-MB-3	F-4	EF-2-2	EF-2-3	ELP-5	EBO-27	E-3
SiO_2	72.66	72.68	73.26	73.3	73.75	73.98	73.99	74.39	75.85	76.33	76.81	77.35	77.89	78.68
TiO_2	0.66	0.44	0.26	0.27	0.82	0.21	0.25	0.35	0.23	0.18	0.16	0.42	0.30	0.44
Al_2O_3	12.38	8.96	14.22	9.20	13.16	8.10	9.49	9.11	14.31	13.42	13.31	10.26	9.35	8.77
Fe_2O_3t	5.80	9.63	2.81	5.92	1.76	10.05	5.75	7.12	0.21	1.10	0.45	4.53	4.66	4.94
MgO	0.01	0.18	0.11	0.05	0.02	0.04	0.02	0.65	0.01	0.04	0.02	0.12	0.14	0.45
CaO	0.04	0.09	0.09	0.24	0.03	0.03	0.10	0.06	0.10	0.08	0.07	0.08	0.05	0.19
MnO	0	0.04	0.05	0.05	0.03	0.05	0.07	0.10	0	0.01	0.01	0.01	0.08	0.03
Na_2O	6.79	2.03	6.46	4.57	4.49	2.15	4.58	1.54	8.10	7.59	7.55	2.87	2.37	3.53
K_2O	0.19	4.28	1.08	4.55	4.09	3.59	4.39	3.52	0.16	0.06	0.09	2.05	3.00	1.19
P_2O_5	0.05	0.01	0.03	0.02	0.03	0.02	0.02	0.02	0.03	0.02	0.02	0.02	0.02	0.07
LOI	0.56	0.71	1.01	0.84	0.98	1.07	0.56	2.19	0.49	0.70	0.67	1.61	1.27	0.94
Total	99.14	99.05	99.38	99.01	99.16	99.29	99.22	99.05	99.49	99.53	99.16	99.32	99.13	99.23
Percent oxides recalculated on a volatile-free basis														
SiO_2	73.71	73.91	74.47	74.67	75.12	75.32	74.99	76.80	76.62	77.23	77.99	79.16	79.59	80.05
TiO_2	0.67	0.45	0.26	0.28	0.84	0.21	0.25	0.36	0.23	0.18	0.16	0.43	0.31	0.45
Al_2O_3	12.56	9.11	14.46	9.37	13.40	8.25	9.62	9.41	14.45	13.58	13.51	10.50	9.55	8.92
Fe_2O_3t	5.88	9.79	2.86	6.03	1.79	10.23	5.83	7.35	0.21	1.11	0.46	4.64	4.76	5.03
MgO	0.01	0.18	0.11	0.05	0.02	0.04	0.02	0.67	0.01	0.04	0.02	0.12	0.14	0.46
CaO	0.04	0.09	0.09	0.24	0.03	0.03	0.10	0.06	0.10	0.08	0.07	0.08	0.05	0.19
MnO	0.00	0.04	0.05	0.05	0.03	0.05	0.07	0.10	0.00	0.01	0.01	0.01	0.08	0.03
Na_2O	6.89	2.06	6.57	4.66	4.57	2.19	4.64	1.59	8.18	7.68	7.67	2.94	2.42	3.59
K_2O	0.19	4.35	1.10	4.63	4.17	3.66	4.45	3.63	0.16	0.06	0.09	2.10	3.07	1.21
P_2O_5	0.05	0.01	0.03	0.02	0.03	0.02	0.02	0.02	0.03	0.02	0.02	0.02	0.02	0.07
Total	100	100	100	100	100	100	100	100	100	100	100	100	100	100

Notes: Major element oxides in wt.%. Fe_2O_3, total Fe. People interested in knowing the exact geographical location of the samples may get in contact with M. Etxebarria for a detailed map.

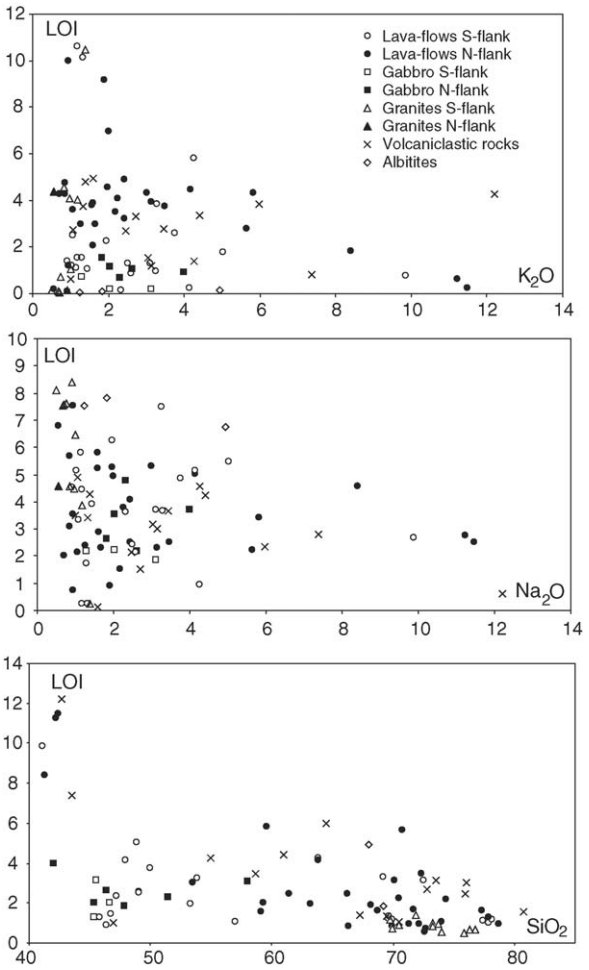

Fig. 10. Loss on ignition (LOI) vs. SiO_2, Na_2O and K_2O.

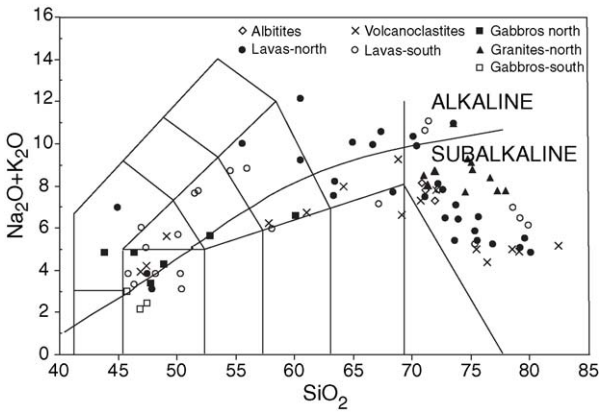

Fig. 11. Total alkali vs. silica diagram for samples of volcanics and intrusives from both flanks. The dark solid line corresponds to the Irvine and Baragar (1971) boundary.

Prat and Girbacea, 2000; Best and Christiansen, 2001). Besides, as gabbros and basalts (*sensu lato*) of the N flank show the same compositional variations, gabbros would not represent cumulates but "frozen melts" (Chalot-Prat et al., 2003).

The direct correlation between silica and alkali in the S flank basalts may trace fractional crystallization of the eruptive basaltic liquids. Because their alkali, TiO_2 and P_2O_5 contents are not negligible but somewhat lower than in the northern flank, their mantle source was likely located in the subcontinental mantle, somewhat less metasomatized than on the northern flank.

The very homogeneous composition of gabbros of the S flank, with higher CaO and much lower Na_2O, K_2O and TiO_2 contents than basalts, suggests they came from crystallization of magma injections distinct from those giving the volcanics. This alkali-depleted parent magma could have a composition close to that of the source of Mid-Oceanic Ridge Basalts (MORB), i.e. residual and not metasomatized as the asthenospheric mantle (Chalot-Prat et al., 2003; Chalot-Prat, 2005).

As the gabbros were emplaced somewhat later than the volcanics on both flanks, it is suggested that, if the involved mantle source did not change with time on the N flank, it changed and became much deeper on the S flank. However, in absence of any trace element data, it cannot be excluded that this difference between basalts and gabbros from the S flank could originate from an increase, with time, of the partial melting degree of the same metasomatized mantle source.

Overall, the felsic set is clearly distinct from the mafic set. The large compositional gap between both sets, with a very small intermediate group in between both, argues against the origin of felsic magmas by fractional crystallization of the basaltic ones. The felsic set instead likely originated from partial melting of the continental crust, as implied by the diverse, significant negative correlations between SiO_2 and all the other elements, alkali included as far as alteration did not play any major role (Chalot-Prat, 1995). Indeed the obvious positive correlation between alkalis, TiO_2, Fe_2O_3, Al_2O_3, CaO and MgO (the latter two only in the N flank), suggests that partial melting of silica poor minerals, such as amphibole and perhaps phlogopite as in the subcontinental mantle, would have partly controlled the composition of melts, with crustal source heterogeneity contributing to the greater diversity of the felsic set.

The albitites are unusual, with clearly higher contents in Na_2O, and somewhat lower K_2O than gabbros, reflecting a composition close to the Mid-Oceanic Ridge plagiogranites (Costa and Caby, 2001; Chalot-Prat, unpublished data on MOR albitites). They may have been generated through partial melting of tholei-

Table 2
Representative major element analysis of Cambrian volcaniclastic rocks from the both flanks of the Monesterio Antiform (SF = south flank)

Rock name	Tephrite	Tephrite	Trachyandesite	Trachyandesite	Trachyandesite	Dacite	Trachyte	Dacite	Dacite	Dacite	Dacite	Rhyolite	Rhyolite	Rhyolite	Basalt SF
Sample	EG-IG	EG-PI	EG-MB-4	EG-LM-2	EG-KA-1	EG-KA-4	EFE-25	E-16	E-17	EG-TO-1	EG-LM-5	EG-TO-2	EG-KA-3	EG-CA-3	EG-FB-8
SiO_2	42.69	43.50	55.00	58.64	61.02	64.49	67.27	69.44	70.52	72.84	73.54	75.93	76.06	80.71	46.97
TiO_2	3.90	3.81	3.16	1.77	0.58	0.65	0.68	0.47	0.50	0.58	0.44	0.42	0.71	0.45	3.31
Al_2O_3	14.26	14.31	12.68	13.64	16.19	12.4	13.25	12.28	12.93	13.96	8.73	12.06	9.24	10.76	14.33
Fe_2O_3t	13.58	14.92	11.02	9.70	8.09	6.07	7.09	8.35	5.94	3.44	7.18	2.76	2.92	0.55	14.14
MgO	2.25	6.53	2.7	2.52	0.79	1.31	0.05	0.38	0.26	0.79	0.94	0.67	0.52	0.28	6.40
CaO	4.56	5.42	3.32	2.69	0.81	2.01	0.06	0.07	0.13	0.14	1.20	0.13	1.55	0.10	9.00
MnO	0.30	0.18	0.10	0.10	0.06	0.15	0.29	0.01	0.01	0.01	0.14	0	0.07	0	0.24
Na_2O	0.62	2.81	4.56	3.67	4.23	2.34	4.26	3.42	4.90	1.52	3.00	2.13	3.17	0.11	3.51
K_2O	4.29	0.84	1.39	2.79	3.36	3.83	4.79	3.73	2.72	3.31	1.20	2.69	1.55	4.96	0.64
P_2O_5	0.59	0.52	1.34	0.56	0.08	0.19	0.06	0.06	0.08	0.06	0.03	0.02	0.43	0.09	0.62
LOI	12.2	7.37	4.26	3.45	4.41	5.97	1.39	1.32	1.06	2.71	3.14	2.47	3.04	1.59	1.01
Total	99.24	100.21	99.53	99.53	99.61	99.41	99.19	99.53	99.05	99.36	99.54	99.28	99.27	99.60	100.17
Percent oxides recalculated on a volatile-free basis															
SiO_2	49.05	46.85	57.73	61.03	64.10	69.02	68.78	70.71	71.97	75.36	76.29	78.43	79.04	82.35	47.37
TiO_2	4.48	4.10	3.32	1.84	0.61	0.70	0.70	0.48	0.51	0.60	0.46	0.43	0.74	0.46	3.34
Al_2O_3	16.38	15.41	13.31	14.20	17.01	13.27	13.55	12.50	13.20	14.44	9.06	12.46	9.60	10.98	14.45
Fe_2O_3t	15.60	16.07	11.57	10.10	8.50	6.50	7.25	8.50	6.06	3.56	7.45	2.85	3.03	0.56	14.26
MgO	2.59	7.03	2.83	2.62	0.83	1.40	0.05	0.39	0.27	0.82	0.98	0.69	0.54	0.29	6.45
CaO	5.24	5.84	3.48	2.80	0.85	2.15	0.06	0.07	0.13	0.14	1.24	0.13	1.61	0.10	9.08
MnO	0.34	0.19	0.10	0.10	0.06	0.16	0.30	0.01	0.01	0.01	0.15	0.00	0.07	0.00	0.24
Na_2O	0.71	3.03	4.79	3.82	4.44	2.50	4.36	3.48	5.00	1.57	3.11	2.20	3.29	0.11	3.54
K_2O	4.93	0.90	1.46	2.90	3.53	4.10	4.90	3.80	2.78	3.42	1.24	2.78	1.61	5.06	0.65
P_2O_5	0.68	0.56	1.41	0.58	0.08	0.20	0.06	0.06	0.08	0.06	0.03	0.02	0.45	0.09	0.63
Total	100	100	100	100	100	100	100	100	100	100	100	100	100	100	100

Notes: Major element oxides in wt.%. Fe_2O_3, total Fe. People interested in knowing the exact geographical location of the samples may get in contact with M. Etxebarria.

Table 3
Representative major element analysis of Cambrian igneous rocks from the southern flank of the Monesterio Antiform

Rock name	Tephrite	Gabbro	Gabbro	Basalt	Trachybasalt	Gabbro	Basalt	Basalt	Trachybasalt	Basaltic trachyandesite	Basalt	Basalt	Basaltic trachyandesite	Basaltic trachyandesite	Basaltic trachyandesite	Basaltic andesite
Sample	689	EG-G-1	EG-G-3	EG-FB-2	EG-FB-7	EG-FR-1	EG-GD-1	EG-FB-3	EG-BO-2	EG-BO-3	AR-96-7B	AR-96-7	LE-97-16	GT-18	GT-9	EG-FB-11
SiO_2	41.15	45.34	45.52	45.80	46.39	46.65	46.7	47.17	47.95	48.85	49.02	49.09	49.95	53.32	53.89	56.97
TiO_2	4.84	2.72	0.63	1.04	2.96	1.17	3.21	2.32	3.13	2.20	0.71	0.65	2.20	1.42	1.54	1.49
Al_2O_3	12.33	14.9	19.22	14.7	17.48	18.01	19.21	15.11	15.26	17.98	19.05	14.02	19.45	17.42	16.91	15.59
Fe_2O_3t	14.38	11.6	7.11	12.11	12.39	9.71	10.5	11.06	12.89	7.13	10.57	10.31	8.15	9.06	8.92	8.95
MgO	3.58	7.60	10.8	13.25	6.03	8.05	3.62	7.41	4.17	6.27	4.07	9.11	7.41	3.55	1.82	3.57
CaO	9.40	13.6	11.75	8.40	6.84	12.02	9.73	10.5	6.07	4.82	10.62	10.4	1.45	3.91	3.60	4.29
MnO	0.17	0.16	0.12	0.14	0.27	0.18	0.14	0.12	0.26	0.10	0.14	0.19	0.08	0.28	0.14	0.39
Na_2O	2.67	2.2	1.84	1.74	4.51	2.22	3.92	3.61	5.15	5.47	2.14	2.41	4.87	6.25	7.51	3.35
K_2O	0.77	0.73	0.21	1.53	1.41	0.17	1.05	0.15	0.25	1.78	0.86	1.31	2.60	2.28	0.96	2.49
P_2O_5	0.52	0.16	0.04	0.10	0.53	0.11	0.52	0.42	0.53	0.31	0.14	0.14	0.31	0.24	0.96	0.97
LOI	9.87	1.30	3.13	1.30	0.92	2.04	1.44	2.33	4.15	5.03	2.60	2.51	3.77	1.96	3.27	1.08
Total	99.68	100.31	100.37	100.11	99.73	100.33	100.04	100.2	99.81	99.94	99.92	100.14	100.24	99.69	99.52	99.14
Percent oxides recalculated on a volatile-free basis																
SiO_2	45.82	45.79	46.81	46.35	46.95	47.46	47.36	48.20	50.13	51.47	50.37	50.28	51.78	54.56	55.99	58.10
TiO_2	5.39	2.75	0.65	1.05	3.00	1.19	3.26	2.37	3.27	2.32	0.73	0.67	2.28	1.45	1.60	1.52
Al_2O_3	13.73	15.05	19.77	14.88	17.69	18.32	19.48	15.44	15.95	18.94	19.57	14.36	20.16	17.82	17.57	15.90
Fe_2O_3t	16.01	11.72	7.31	12.26	12.54	9.88	10.65	11.30	13.47	7.51	10.86	10.56	8.45	9.27	9.27	9.13
MgO	3.99	7.68	11.11	13.41	6.10	8.19	3.67	7.57	4.36	6.61	4.18	9.33	7.68	3.63	1.89	3.64
CaO	10.47	13.74	12.08	8.50	6.92	12.23	9.87	10.73	6.35	5.08	10.91	10.65	1.50	4.00	3.74	4.37
MnO	0.19	0.16	0.12	0.14	0.27	0.18	0.14	0.12	0.27	0.11	0.14	0.19	0.08	0.29	0.15	0.40
Na_2O	2.97	2.22	1.89	1.76	4.56	2.26	3.98	3.69	5.38	5.76	2.20	2.47	5.05	6.40	7.80	3.42
K_2O	0.86	0.74	0.22	1.55	1.43	0.17	1.06	0.15	0.26	1.88	0.88	1.34	2.70	2.33	1.00	2.54
P_2O_5	0.58	0.16	0.04	0.10	0.54	0.11	0.53	0.43	0.55	0.33	0.14	0.14	0.32	0.25	1.00	0.99
Total	100	100	100	100	100	100	100	100	100	100	100	100	100	100	100	100

Rock name	Dacite	Albitite	Albitite	Dacite	Albitite	Dacite	Rhyolite	Rhyolite	Rhyolite	Rhyolite	Rhyolite
Sample	682	EG-ALB-2	EG-ALB-3	687	EG-ALB-1	681	683	686	EG-BO-5	EG-BO-6	688
SiO_2	63.80	68.01	69.20	69.24	69.57	72.48	69.63	69.96	77.45	77.92	78.20
TiO_2	0.92	0.53	0.66	0.67	0.73	0.44	0.26	0.76	0.10	0.11	0.28
Al_2O_3	21.07	11.95	13.47	14.39	12.98	9.79	13.66	15.69	12.45	12.53	9.99
Fe_2O_3t	1.48	2.40	4.04	3.17	3.73	7.65	3.78	0.52	0.47	0.44	3.15
MgO	0.74	1.53	0.09	0.50	0.80	0.32	0.12	0.2	0.91	0.95	0.05
CaO	0.13	3.20	2.18	0.21	2.32	0.36	0.04	0.04	0.30	0.11	0.04
MnO	0.01	0.07	0.01	0.10	0.03	0.16	0.01	0	0	0	0.18
Na_2O	0.95	6.73	7.82	3.65	7.55	3.72	0.24	0.24	5.80	5.16	4.45
K_2O	5.81	0.15	0.11	3.84	0.07	1.30	10.14	10.59	1.09	1.22	1.56
P_2O_5	0.05	0.03	0.17	0.10	0.17	0.02	0.04	0.05	0.01	0.01	0.03
LOI	4.27	4.93	1.83	3.29	1.24	3.12	1.33	1.18	1.14	1.03	1.17
Total	99.23	99.53	99.58	99.16	99.19	99.36	99.25	99.23	99.72	99.48	99.10
Percent oxides recalculated on a volatile-free basis											
SiO_2	67.19	71.89	70.79	72.22	71.03	75.31	71.11	71.35	78.57	79.15	79.85
TiO_2	0.97	0.56	0.68	0.70	0.75	0.46	0.27	0.78	0.10	0.11	0.29
Al_2O_3	22.19	12.63	13.78	15.01	13.25	10.17	13.95	16.00	12.63	12.73	10.20
Fe_2O_3t	1.56	2.54	4.13	3.31	3.81	7.95	3.86	0.53	0.48	0.45	3.22
MgO	0.78	1.62	0.09	0.52	0.82	0.33	0.12	0.20	0.92	0.96	0.05
CaO	0.14	3.38	2.23	0.22	2.37	0.37	0.04	0.04	0.30	0.11	0.04
MnO	0.01	0.07	0.01	0.10	0.03	0.17	0.01	0.00	0.00	0.00	0.18
Na_2O	1.00	7.11	8.00	3.81	7.71	3.87	0.25	0.24	5.88	5.24	4.54
K_2O	6.12	0.16	0.11	4.01	0.07	1.35	10.36	10.80	1.11	1.24	1.59
P_2O_5	0.05	0.03	0.17	0.10	0.17	0.02	0.04	0.05	0.01	0.01	0.03
Total	100	100	100	100	100	100	100	100	100	100	100

Notes: Major element oxides in wt.%. Fe_2O_3, total Fe. People interested in knowing the exact geographical location of the samples may get in contact with M. Etxebarria.

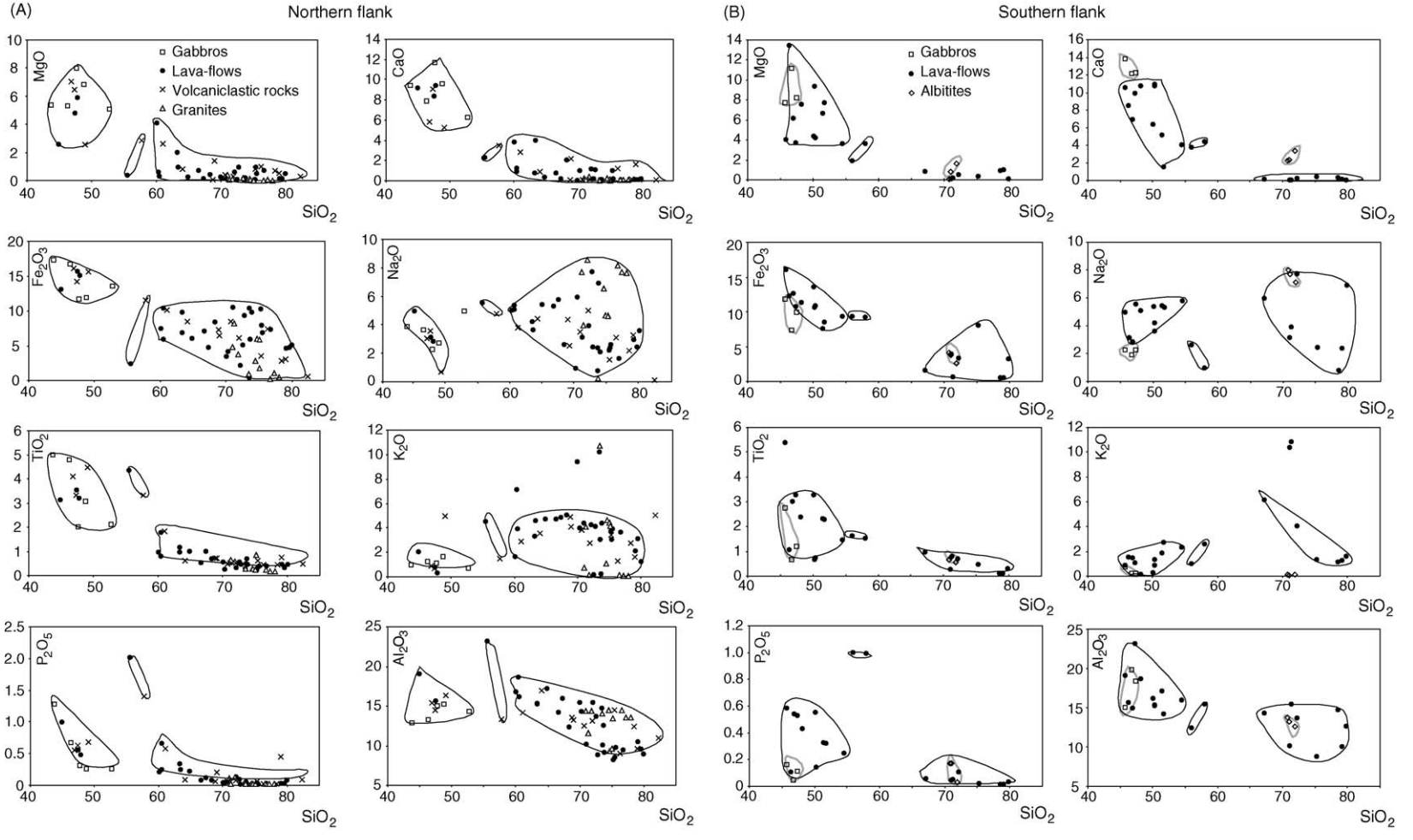

Fig. 12. (A) Harker diagrams for the northern flank. (B) Harker diagrams for the southern flank. Fields around data illlustrate the bimodal distribution of rock types.

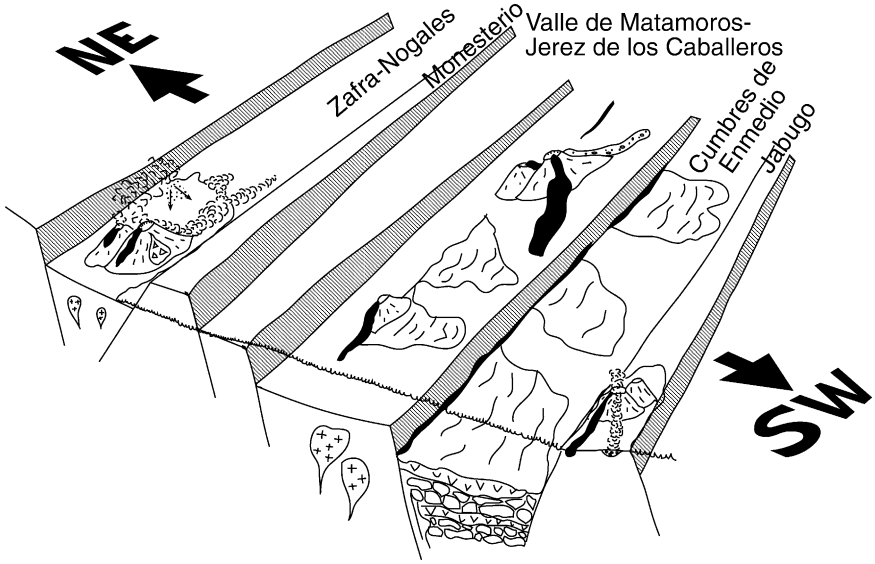

Fig. 13. Paleogeographic reconstruction of the volcanically active passive margin at the end of Cambrian times.

itic gabbros (Costa and Caby, 2001) which were already emplaced within, or underplated below, the continental lower crust. The late emplacement of the albitites relative to the S flank gabbros supports this hypothesis.

The third set of analyses, with two volcanic samples only on each flank, has an intermediate composition in silica (56–58%) and a much higher P_2O_5 contents (up to 1–2%) than other end-members. Its global composition is closer to the mafic set on the S flank, but closer to the felsic set on the N flank. Its specific enrichment in P_2O_5 suggests that a crustal source particularly rich in apatite (or other P-rich minerals) would be a good candidate.

7. Discussion and conclusions

Our detailed study of the Middle to Upper Cambrian magmatism of the Ossa-Morena Zone in relationship with its tectono-sedimentary environment, in the earliest Variscan orogenic cycle in Europe, has brought up a number of new results. They are relevant to the conditions of emplacement, the diversity and the origin of magmas, leading us to recognize a different behavior of the continental lithosphere from the northern to the southern part of the studied areas during the formation of the volcanically active, passive margin of the future Rheic ocean. The formation of this margin lasted from ca. 520–530 Ma (age of the youngest detrital zircon in the Cambrian arkose) and 470–460 Ma (depositional age of the Armorican quartzite) (Gutíerrez-Alonso et al., 2003). The Ossa-Morena Zone rocks in this study thus represent the first volcanic stages associated with the drift between the Armorica Terrane assemblage and Avalonia.

First of all, most of the eruptions were subaerial or occurred under very shallow marine condition in the north, whereas they were always submarine somewhere on a continental shelf in the south. Everywhere, the lateral variations of thickness of the sedimentary deposits document the formation of a passive rifted margin, volcanically active from place to place (Fig. 13). As shallow marine sedimentary deposits predated, accompanied and postdated the volcanic episodes, it is inferred that the basement was subsiding during the whole period of interest. Nevertheless the sudden transition from marine to subaerial environments was due to transient basement uplift episodes, probably related to the buildup of volcanic edifices which was much more efficient northwards because subsidence was less active and the basin was shallower. This can be interpreted in terms of progressive continental crustal thinning inducing rifting and the building of a volcanically active passive margin facing southwards to the future Rheic ocean (Fig. 13). Four volcanic periods happened during transient stages that accompanied an isostatic compensation of the crustal thinning by mantle uplift. The supposed doming led to the formation of fractures allowing magma rising up to the surface. However the existence of numerous sills within the Cambrian sediments means that the fracture propagation was not always so effective. Similar processes occurred but at a larger scale and a deeper level for the emplacement of granites and gabbros. The late-stage emplacement of intrusives relative to the volcanics in both flanks implies that the upper crust became less easy to fracture over time, probably due to thermal softening. The fractures were not randomly distributed, but were

close to each other in the north flank where they allowed the building of large centered edifices on the western side of the coast line. Fractures were mostly scattered in the south flank, giving birth to fissural eruptions and building of basaltic shields.

The composition of magmas is bimodal, with very few samples showing an intermediate composition, suggesting that mantle and crustal sources were involved throughout the volcanic cycle and that mixing processes between mantle and crustal compositions are negligible. The great diversity of felsic magmas probably originated from a very heterogeneous alkali-rich crust. Fractional crystallization relationships appear limited and partial melting relationships prevailed, which means that magmas systematically rose up to the surface after their formation.

The composition of mantle magmas attests to a less metasomatized subcontinental mantle sources towards the south. The youngest southern gabbros document a mantle source close to that of MORB, i.e. depleted and with minimal metasomatization. Partial melting relationships prevailed over fractional crystallization in the northern zone, whereas the reverse case prevailed in the southern zone, perhaps reflecting a faster ascent of mafic magmas northwards.

The causes of mantle and crust partial melting may be influenced by the geodynamic setting. In a post-collisional context, lithospheric thinning is believed to occur in response to the delamination of the thick lithospheric mantle root. During the thinning, the rheological difference between mantle and crust could accommodate a decoupling according to physical processes described in Chalot-Prat and Girbacea (2000 and references therein). The subcontinental mantle would then undergo a crude decompression, which would then trigger an adiabatic partial melting. The mantle melt rose up to the surface if possible or formed subsurface sills and intrusions at deeper levels. As this decoupling depends on heterogeniety, this process could also occur within the subcontinental mantle and/or within the continental crust. The absence of mafic–felsic hybrid rocks leads us to prefer this decoupling process to generate the crustal magmas rather than one in which an ascending mafic magma induces crustal melting.

The fact that both mafic and felsic magma compositions belong to the alkali-rich and silica-saturated series, could be an indication that their sources were genetically related. Indeed the subcontinental mantle is a residual mantle metasomatized by crustal melts (Foley, 1992; Vaselli et al., 1995; Chalot-Prat and Boullier, 1997; Best and Christiansen, 2001; Chalot-Prat et al., 2003). This hypothesis needs to be tested with further studies, including analysis of trace elements and of Nd, Sr and Pb isotopic ratios.

Acknowledgements

This paper reports the main results of the PhD Thesis of M. Etxebarria. This research was performed in the frame of the UPV001-310-EA123/99 and UPV001-310-EA7729/2000 research projects on “Magmatism associated with extensional processes in the Ossa-Morena; I and II” managed by Arturo Apraiz. Reviews by Cristian Pin, John Greenough and Phil McCausland greatly helped to improve and clarify the ideas presented in this contribution.

References

Bard, J.P., 1969. Le métamorphisme régional progressif des Sierras d’Aracena en Andalousie occidentale (Espagne): sa place dans le segment hercynien sud-ibérique. Dr. Sci. Thesis. Univ. Montpellier, USTL, unpublished.

Best, M.G., Christiansen, E.H., 2001. Igneous Petrology. Blackwell Science Eds, 457 pp.

Boillot, G., Coulomb, C., 1998. La déchirure continentale et l’ouverture océanique; Géologie des marges passives. Gordon and Breach Sci. Publ, 208 pp.

Chalot-Prat, F., 1995. Genesis of rhyolitic ignimbrites and lavas from distinct sources at a deep crustal level: field, petrographic, chemical and isotopic (Sr, Nd) constraints in the Tazekka volcanic complex (Eastern Morocco). Lithos 36, 29–49.

Chalot-Prat, F., 2005. An undeformed ophiolite in the Alps: field and geochemical evidences for a link between volcanism and shallow plate tectonic processes. In: Foulger, G.R., Natland, J.H., Presnall, D.C., Anderson, L.D. (Eds.), Plates, Plumes & Paradigms. Geological Society of America, special Paper 388, 751–780.

Chalot-Prat, F., Boullier, A.M., 1997. Metasomatism in the subcontinental mantle beneath the Eastern Carpathians (Romania): new evidence from trace element geochemistry. Contrib. Mineral. Petrol. 129, 284–307.

Chalot-Prat, F., Girbacea, R., 2000. Partial delamination of continental mantle lithosphere, uplift-related crust-mantle decoupling, volcanism and basin formation: a new model for the Pliocene-Quaternary evolution of the southern East-Carpathians, Romania. Tectonophysics 327, 83–107.

Chalot-Prat, F., Ganne, J., Lombard, A., 2003. No significant element transfer from the oceanic plate to the mantle wedge during subduction and exhumation of the Tethys ocean (Western Alps). Lithos 69, 69–103.

Costa, S., Caby, R., 2001. Evolution of the Ligurian Tethys in the Western Alps: Sm/Nd and U/Pb geochronology and rare earth element geochemistry of the Montgenèvre Ophiolite (France). Chem. Geol. 175, 449–466.

Druitt, T.H., Sparks, R.S.J., 1982. A proximal ignimbrite breccia facies on Santorini Greece. J. Volcanol. Geotherm. Res. 13, 147–171.

Eguíluz, L., Apraiz, A., Ábalos, B., Martínez-Torres, L.M., 1995. Évolution de la zone d’Ossa Morena (Espagne) au cours du Protérozöique supérieur: corrélations avec l’orogène cadomien nord armoricain. Géol. France 3, 35–47.

Eguíluz, L., Apraiz, A., Martínez-Torres, L.M., Palacios, T., 1997. Estructura del sector de Zafra: implicaciones en la subdivisión de unidades cámbricas en la Zona de Ossa-Morena (ZOM). Geogaceta 22, 59–62.

Eguíluz, L., Gil Ibarguchi, J.I., Ábalos, B., Apraiz, A., 2000. Superposed Hercynian and Cadomian orogenic cycles in the Ossa-Morena zone and related areas of the Iberian Massif. Bull. Geol. Soc. Am. 112, 1398–1413.

Etxebarria, M., 2003. Reconstrucción geométrica y caracterización petrográfica y geoquímica de los eventos magmáticos y tectónicos cámbricos de la Antiforma de Olivenza-Monesterio, sectores de Zafra-Nogales y Jerez de los Caballeros-Cumbres de Enmedio (Zona de Ossa-Morena). Tesis Universidad del País Vasco.

Etxebarria, M., Apraiz, A., Carracedo, M., 2004. Aportaciones a la geoquímica de rocas básicas cámbricas de la Antiforma de Monesterio (Zona de Ossa-Morena). Geogaceta 34, 99–102.

Fernández-Suárez, J., Gutiérrez-Alonso, G., Jenner, G.A., 2002. The importance of along-margin terrane transport in Northern Gondwana: insights from detrital zircon parentage in Neoproterozoic rocks from Iberia and Brittany. Earth Planet. Sci. Lett. 204, 75–88.

Fernández-Suárez, J., Gutiérrez-Alonso, G., Jenner, G.A., Tubrett, M.N., 2000. New ideas on the Proterozoic-Early Paleozoic evolution of NW Iberia Insights from U–Pb detrital zircon ages. Precambrian Res. 102, 185–206.

Foley, S., 1992. Vein-plus-wall-rock melting mechanisms in the lithosphere and the origin of potassic alkaline magmas. Lithos 28, 435–453.

Franke, W., Dallmeyer, R.D., Weber, K., 1995. Geodynamic evolution. In: Dallmeyer, R.D., Franke, W., Weber, K. (Eds.), Pre-Permian Geology of Central and Western Europe. Springer-Verlag, Berlin/Heidelberg, pp. 579–593.

Friedl, G., Finger, F., McNaughton, N.J., Fletcher, I.R., 2000. Deducing the ancestry of terranes: SHRIMP evidence for South-America-derived Gondwana fragments in central Europe. Geology 28, 1035–1038.

Giese, U., Bühn, B., 1993. Early Paleozoic rifting and bimodal volcanism in the Ossa Morena Zone of south-west Spain. Geol. Rundsch. 83, 143–160.

Gutíerrez-Alonso, G., Fernández-Suárez, J., Jeffries, T.E., Jenner, G.A., Tubrett, M.N., Cox, R., Jackson, S.E., 2003. Terrane accretion and dispersal in the northern Gondwana margin. An early Paleozoic analogue of a long-lived active margin. Tectonophysics 365, 221–232.

Irvine, T.N., Baragar, W.R.A., 1971. A guide to the chemical classification of the common volcanic rocks. Can. J. Earth Sci. 8, 523–548.

Le Maitre, R.W. (Ed.), 1989. A Classification of Igneous Rocks and Glossary of Terms. Blackwell Scientific, Oxford.

Liñán, E., 1978. Bioestratigrafía de la Sierra de Córdoba. Thesis. University of Granada.

Liñán, E., 1984. Introducción al problema de la paleogeografía del Cámbrico de Ossa Morena. Cuad. Lab. Geol. Laxe 8, 283–314.

Liñán, E., Perejón, A., 1981. El Cámbrico inferior de la "Unidad de Alconera" Badajoz (SO de España). Biol. R. Soc. Esp. Hist. Nat. 79, 125–148.

Liñán, E., Fernández-Carrasco, J., 1984. La Formación Torreárboles y la Paleogeografía del límite Cámbrico-Precámbrico en Ossa-Morena (flanco norte de la alineación Olivenza-Monesterio). Cuad. Lab. Geol. Laxe 8, 315–328.

Liñán, E., Quesada, C., 1990. Part V Ossa-Morena zone. 2 Stratigraphy. 2.2. Rift phase (Cambrian). In: Dallmeyer, R.D., Martínez-García, E. (Eds.), Pre-Mesozoic Geology of Iberia. Springer-Verlag, Berlin/Heidelberg, pp. 259–266.

Liñán, E., Gámez-Vintáned, J.A., 1993. Lower Cambrian paleogeography of the Iberian península and its relations with some neighbouring European areas. Bull. Soc. Géol. Fr. 164, 831–842.

Liñán, E., Palacios, F., Perejón, A., 1984. Precambrian–Cambrian boundary and correlation from southwestern and central part of Spain. Geol. Mag. 121, 221–228.

Liñán, H., Gonçalves, F., Gámez Vintáned, J.A., Gonzalo, R., 1997. Evolución paleogeográfica del Cámbrico de la zona de Ossa-Morena basada en el registro fósil. In: Araujo, A.A., Pereira, M.F. (Eds.), Estudos sobre a geologia da Zona de Ossa-Morena (Maciço Ibérico). Livro de homenagem ao Prof. Francisco Gonçalves, Evora, pp. 1–26.

Mata, J., Munhá, J., 1986. Tectonic setting of magmatic activity in southern branch of the Iberian Variscan Chain. Maleo 2, 13–28.

Mata, J., Munhá, J., 1990. Magmatogénese de metavulcanitos câmbricos do Nordeste Alentejano: os estados iniciais do "rifting" continental. Com. Serv. Geol. Portugal 74, 61–89.

Mc Cann, T., Saintot, A., Chalot-Prat, F., Kitchka, A, Fokin, P., Alekseev, A., Europrobe INTAS Research Team, 2003. Evolution of the southern margin of the Donbass (Ukraine) from Devonian to Early Carboniferous times. In: Mc Cann, T., Saintot, A. (Eds.), Tracing Tectonic Deformation Using the Sedimentary Record, vol. 208. Geological Society, London, Special Publications, pp. 117–135.

McPhie, J., Doyle, M., Allen, R., 1993. Volcanic Textures. A Guide to the Interpretation of Textures in Volcanic Rocks. Codes Key Centre, Univ. Tasmania.

Muelas, A., Soubrier, J., Hernández, J.L., 1977. Mapa geológico Nacional (MAGNA), mapa y memoria explicativa de la Hoja No. 853 (Burguillos del Cerro). Instituto Geológico y Minero de España (IGME), scale 1:50.000.

Murphy, J.B., Strachan, R.A., Nance, R.D., Parker, K.D., Fowler, M.B., 2000. Proto-Avalonia: A 1 2-1. 0 Ga tectonothermal event and constraints for the evolution of Rodinia. Geology 28, 1071–1074.

Murphy, J.B., Eguíluz, L., Zulauf, G., 2002. Cadomian Orogens, peri-Gondwanan correlatives and Laurentia-Baltica connections. Tectonophysics 352, 1–9.

Murphy, J.B., Pisarevsky, S.A., Nance, R.D., Keppie, J.D., 2004. Neoproterozoic-early Paleozoic evolution of peri-Gondwanan terranes: Implications for Laurentia-Gondwana connections. Int. J. Earth Sci. 93, 659–682.

Nägler, T., 1990. Sm–Nd, Rb–Sr and common lead isotope geochemistry on fine-grained sediments of the Iberian Massif. Ph.D. Thesis. ETH Zürich, unpublished.

Ochsner, A., 1993. U–Pb Geochronology of the Upper Proterozoic-Lower Paleozoic geodynamic evolution in the Ossa-Morena Zone (SW Iberia): Constraints on the timing of the cadomian orogeny. Ph.D. Dissertation. Eidgenössische Technische Hoschschule, Zürich, 10.392, 430 pp.

Ordóñez, B. 1998. Geochronological studies of the Pre-Mesozoic basement of the Iberian Massif: the Ossa Morena zone and the Allochthonous Complexes within the Central Iberian zone. Ph.D. Dissertation. Eidgenössische Technische Hoschschule, Zürich, 12.940, pp. 1–235.

Palmer, A.R., James, N.P., 1980. The Hawke Bay event: a circum-Iapetus regression near the Lower–Middle Cambrian boundary. In: Wones, D.R. (Ed.), The Caledonides in USA, vol. 2. Virginia Polytech. Inst. and State Univ., Memoir, pp. 15– 18.

Pecerillo, A., 1999. Multiple mantle metasomatism in central-southern Italy: geochemical effects, timing and geodynamic implications. Geology 27, 315–318.

Pecerillo, A., Panza, G.F., 1999. Upper mantle domains beneath central-southern Italy: petrological, geochemical and geophysical constraints. Pure Appl. Geophys. 156, 421–443.

Perejón, A., Moreno-Eiris, E., 1992. Paleozoico Inferior de Ossa Morena. In: Gutiérrez, J.G., Saavedra, J., Rábano, I. (Eds.), Paleozoico Inferior de Ibero-América, Univ. Extremadura, pp. 557–565.

Quesada, C., Apalategui, O., Eguíluz, L., Liñán, E., Palacios, T., 1990. Ossa-Morena Zone: Precambrian. In: Dallmeyer, R.D., Martínez-García, E. (Eds.), Pre-Mesozoic Geology of Iberia. Springer-Verlag, Berlin/Heidelberg, pp. 250–258.

Roso de Luna, I., Hernández-Pacheco, F., 1955. Mapa geológico Nacional (MAGNA), mapa y memoria explicativa de la Hoja No. 854 (Zafra). Instituto Geológico y Minero de España (IGME), scale 1:50.000.

Sagredo, J., Peinado, M., 1992. Vulcanismo Cámbrico de la Zona de Ossa-Morena. In: Gutierrez Marco, J.G., Saavedra, J., Rábano, I. (Eds.), Paleozoico Inferior de Ibero-América. Univ. Extremadura, pp. 567–575.

Sánchez García, T., Bellido, F., Quesada, C., 2003. Geodynamic setting and geochemical signatures of Cambrian-Ordovician rift-related igneous rocks (Ossa-Morena Zone SW Iberia). Tectonophysics 365, 233–255.

Sánchez-Carretero, R., Carracedo, M., Eguíluz, L., Alonso, A., 1999. Magmatismo alcalino tardicadomiense en la zone de Ossa Morena (Macizo Ibérico): cartografía, petrografía y geoquímica preliminar del macizo de Almendral. Geogaceta 26, 87–91.

Sparks, R.S.J., Self, S., Walker, G.P.L., 1973. Products of ignimbrite eruptions. Geology 1, 115–118.

Tichomirowa, M., Berger, H.J., Koch, E.A., Belyatski, B.V., Götze, J., Kempe, U., Nasdala, L., Schaltegger, U., 2001. Zircon ages of high-grade gneisses in the eastern Erzgebirge (central European Variscides)-constraints on origin of the rocks and Precambrian to Ordovician magmatic events in the Variscan foldbelt. Lithos 56, 303–332.

Vaselli, O., Downes, H., Thirlwall, M., Dobosi, G., Coradossi, N., Seghedi, I., Szakacs, A., Vannucci, R., 1995. Ultramafic xenoliths in Plio-Pleistocene alkali basalts from the eastern Transylvanian Basin: depleted mantle enriched by vein metasomatism. J. Petrol. 36, 23–53.

Wilson, M., 1989. Igneous Petrogenesis: a Global Tectonic Approach. Unwin Hyman, London, 466 pp.

Winter, J.D., 2001. An Introduction to Igneous and Metamorphic Petrology. Prentice Hall, 697 pp.